Cell

Proteostasis governs differential temperature sensitivity across embryonic cell types

Graphical abstract

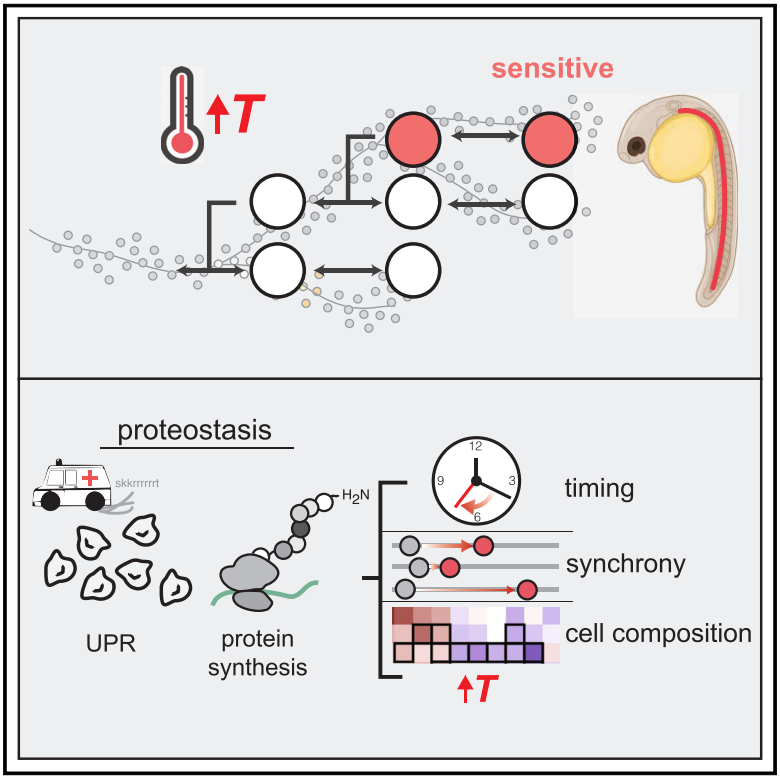

Authors

Michael W. Dorrity, Lauren M. Saunders, Madeleine Duran, ..., David W. Raible, David Kimelman, Cole Trapnell

Correspondence

dorrity@embl.de (M.W.D.), coletrap@uw.edu (C.T.)

In brief

Embryo-wide profiling of transcription, timing, and cell composition in zebrafish reveals processes that limit developmental robustness under increasing temperatures.

Highlights

- Individual-level scRNA quantifies variability in embryogenesis
- Digital embryo staging permits time-controlled statistical analysis
- Temperature accelerates developmental rate non-uniformly across cell types
- Sensitivity of notochord sheath cells via UPR-dependent control of proteostasis

Dorrity et al., 2023, Cell *186*, 5015–5027
November 9, 2023
https://doi.org/10.1016/j.cell.2023.10.013

CellPress

Cell

CellPress
OPEN ACCESS

Article

Proteostasis governs differential temperature sensitivity across embryonic cell types

Michael W. Dorrity,[1,2,*] Lauren M. Saunders,[1] Madeleine Duran,[1] Sanjay R. Srivatsan,[1] Eliza Barkan,[1] Dana L. Jackson,[1] Sydney M. Sattler,[1] Brent Ewing,[1] Christine Queitsch,[1] Jay Shendure,[1,5,6] David W. Raible,[4] David Kimelman,[3] and Cole Trapnell[1,7,*]

[1]Department of Genome Sciences, University of Washington, Seattle, WA 98195, USA
[2]Structural and Computational Biology, European Molecular Biology Laboratory, 69117 Heidelberg, Germany
[3]Department of Biochemistry, University of Washington, Seattle, WA 98195, USA
[4]Department of Biological Structure, University of Washington, Seattle, WA 98195, USA
[5]Brotman Baty Institute for Precision Medicine, Seattle, WA 98195, USA
[6]Howard Hughes Medical Institute, Seattle, WA 98195, USA
[7]Lead contact
*Correspondence: dorrity@embl.de (M.W.D.), coletrap@uw.edu (C.T.)
https://doi.org/10.1016/j.cell.2023.10.013

SUMMARY

Embryonic development is remarkably robust, but temperature stress can degrade its ability to generate animals with invariant anatomy. Phenotypes associated with environmental stress suggest that some cell types are more sensitive to stress than others, but the basis of this sensitivity is unknown. Here, we characterize hundreds of individual zebrafish embryos under temperature stress using whole-animal single-cell RNA sequencing (RNA-seq) to identify cell types and molecular programs driving phenotypic variability. We find that temperature perturbs the normal proportions and gene expression programs of numerous cell types and also introduces asynchrony in developmental timing. The notochord is particularly sensitive to temperature, which we map to a specialized cell type: sheath cells. These cells accumulate misfolded protein at elevated temperature, leading to a cascading structural failure of the notochord and anatomic defects. Our study demonstrates that whole-animal single-cell RNA-seq can identify mechanisms for developmental robustness and pinpoint cell types that constitute key failure points.

INTRODUCTION

Temperature and developmental rate are commonly correlated across animal development.[1–3] The acceleration of development at higher temperatures has been attributed to increased metabolic rate and protein synthesis.[4] Within a species-specific tolerated range, embryos raised in elevated temperatures are phenotypically normal, suggesting that the developmental program is synchronously accelerated. While the mechanisms underlying this synchrony are not fully understood, recent studies have emphasized the role of proteostasis—the maintenance of proper protein folding, synthesis, and degradation of proteins—in determining developmental rate differences across species.[5–7] Mechanisms regulating cellular proteostasis are also key for understanding the relationship between environmental stress and phenotype.[8] Regulation of protein folding and synthesis is sensitive to diverse environmental signals,[9] and misregulation of these processes has phenotypic consequences.[10–13] Because the burden of proteostasis varies considerably across cell types,[14,15] we sought to use transcriptional signatures of proteostasis to investigate how each lineage is able to buffer the effects of temperature stress. Perturbation of proteostasis during early development introduces phenotypic variability,[13,16,17] but these phenotypes are non-random, suggesting that some cell types or developmental processes may be more sensitive to stress than others.

Zebrafish embryos are naturally exposed to temperature fluctuation and display temperature-induced phenotypes and alterations in developmental rate. Furthermore, temperature influences body size scaling, presumably through coordinated effects on the program of development,[18] and also has consequences for aging. While the extended lifespan of zebrafish makes aging studies challenging, fast-growing annual killifish show reduced lifespan when raised at elevated temperature.[19] Wild populations of *Danio rerio* have a natural range spanning from 26°C to as high as 38°C.[20] In lab populations of zebrafish, embryos cannot survive chronic exposure to 36°C and beyond, while they display an increasing number of phenotypic abnormalities from 32°C and beyond.[1] This phenomenon is not limited to ectotherms; thermal limits are evident in mammals and other vertebrates, with species-specific differences defining the critical temperature thresholds beyond which developmental phenotypes arise.[21,22]

We sought to understand the cellular basis for stress-induced developmental phenotypes and, specifically, whether cell types

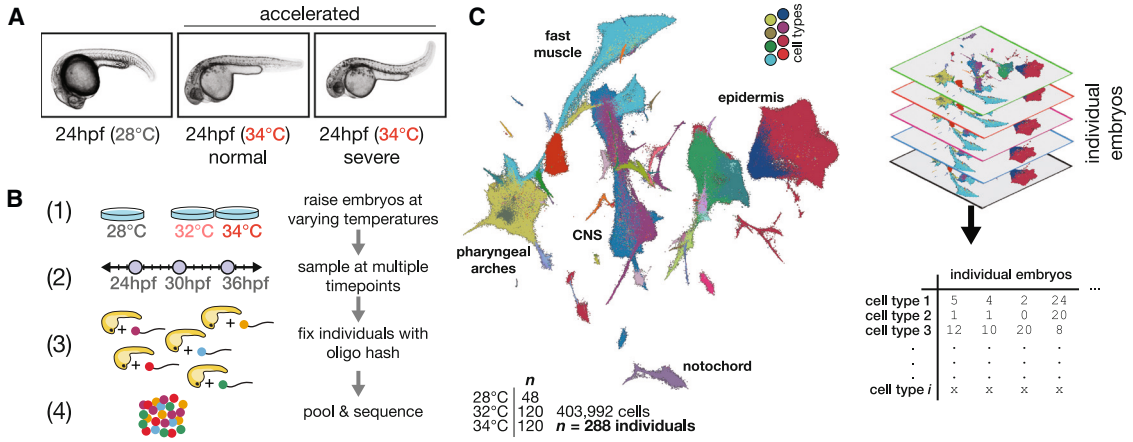

Figure 1. Effects of stress on phenotypic variability are captured via individual animal hashing of single-cell transcriptomes

(A) Representative images of 24 hpf embryos raised at standard and elevated temperature; individual embryos with normal-looking and bent-tail phenotypes were included in the dataset.

(B) Experimental workflow for temperature perturbation experiment and individual embryo hashing.

(C) Uniform manifold approximation and projection (UMAP) of temperature-perturbation dataset, projected into coordinate space of reference atlas (see Saunders et al.[32]). Right side shows how single-cell data are transformed to generate cell composition matrices.

respond differently to temperature. Single-cell genomic techniques can resolve heterogeneity in developmental timing and in levels of molecular processes promoting proteostasis across cell types, but these techniques are limited in their ability to capture variability in the form of biological replicates because of the standard practice of pooling embryos. To overcome this, we use single-cell combinatorial indexing (sci-RNA-seq) combined with DNA oligo hashing to capture transcriptional states and cell type abundances for hundreds of individual zebrafish embryos at multiple temperatures and time points. We leverage this large number of replicates to make statistical inferences about the drivers of environmentally induced phenotypes as well as to identify molecular sources and cell-type-specific contributions to the loss of developmental robustness. From these analyses, we find that temperature affects both developmental rate and synchrony among cell types and that the unfolded protein response (UPR) is required for temperature-induced acceleration. Furthermore, temperature stress alters cell type composition, leaving a lasting imprint on the embryo that cannot be explained by differences in developmental stage. Finally, we show that perturbed proteostasis reveals cell-type-specific temperature sensitivity in the notochord. Taken together, we identify cell-type-specific mechanisms of developmental robustness by integrating individual-to-individual variation and accounting for differential responses to temperature across cell types.

RESULTS

Multiplexed single-cell RNA-seq profiles individual embryos developing under temperature stress

To measure the effects of temperature on developmental robustness, we raised zebrafish embryos over a range of increasingly stressful temperatures below the threshold for heat shock.[23] In addition to the standard temperature of 28°C, we raised embryos in the standard condition, as well as at two elevated temperatures, 32°C and 34°C. At elevated temperatures, embryos developed at a faster rate,[24] with a substantial fraction of individuals showing axial defects of varying severity, along with other previously documented phenotypes (Figure 1A).[1,25–27] Because we can profile individuals, we included embryos raised at elevated temperatures that either were phenotypically normal or had severe, temperature-induced phenotypes. To identify individual embryos, we used nuclear "hashing" wherein polyadenylated DNA oligos with unique barcodes for each embryo are added and fixed along with nuclei after whole-embryo dissociation (Figure 1B; Methods S1).[28] To account for increased variability in elevated temperature samples, we sampled additional embryos in these conditions (16 28°Ccontrol, 40 32°C, and 40 34°C embryos from each time point). Treated and control embryos from three time points (24, 30, 36 hours postfertilization [hpf]) were dissociated and hashed individually and subsequently processed with a single-cell combinatorial indexing (sci) protocol to isolate single nuclei with quality comparable to previous sci-RNA-seq experiments (Figures S1A and S1B) for transcriptome profiling.[29] We recovered 5%–10% of the cells (Figures S1A–S1C) from each individual embryo profiled (assuming 20,000–40,000 cells per embryo), which was sufficient to capture all major cell types for each individual. Cell types were represented more evenly (Gini index = 0.67) than in previous whole-embryo studies (Gini index = 0.80 and 0.71 for atlases from Wagner et al.[30] and Farnsworth et al.,[31] respectively), possibly owing to our use of single-nucleus rather than whole-cell RNA-seq (Figure S1D). By combining the data from all 288 profiled individuals (403,992 total cells), we built a comprehensive atlas of cell-type-specific responses to temperature stress (Figure 1C). We projected our temperature perturbation data onto our annotated zebrafish development reference dataset produced from analyzing 1.2 million cells from 18 hpf to 96 hpf (see Saunders et al.[32]) and identified 85 distinct cell types at these stages. Consistent with the robust progression of

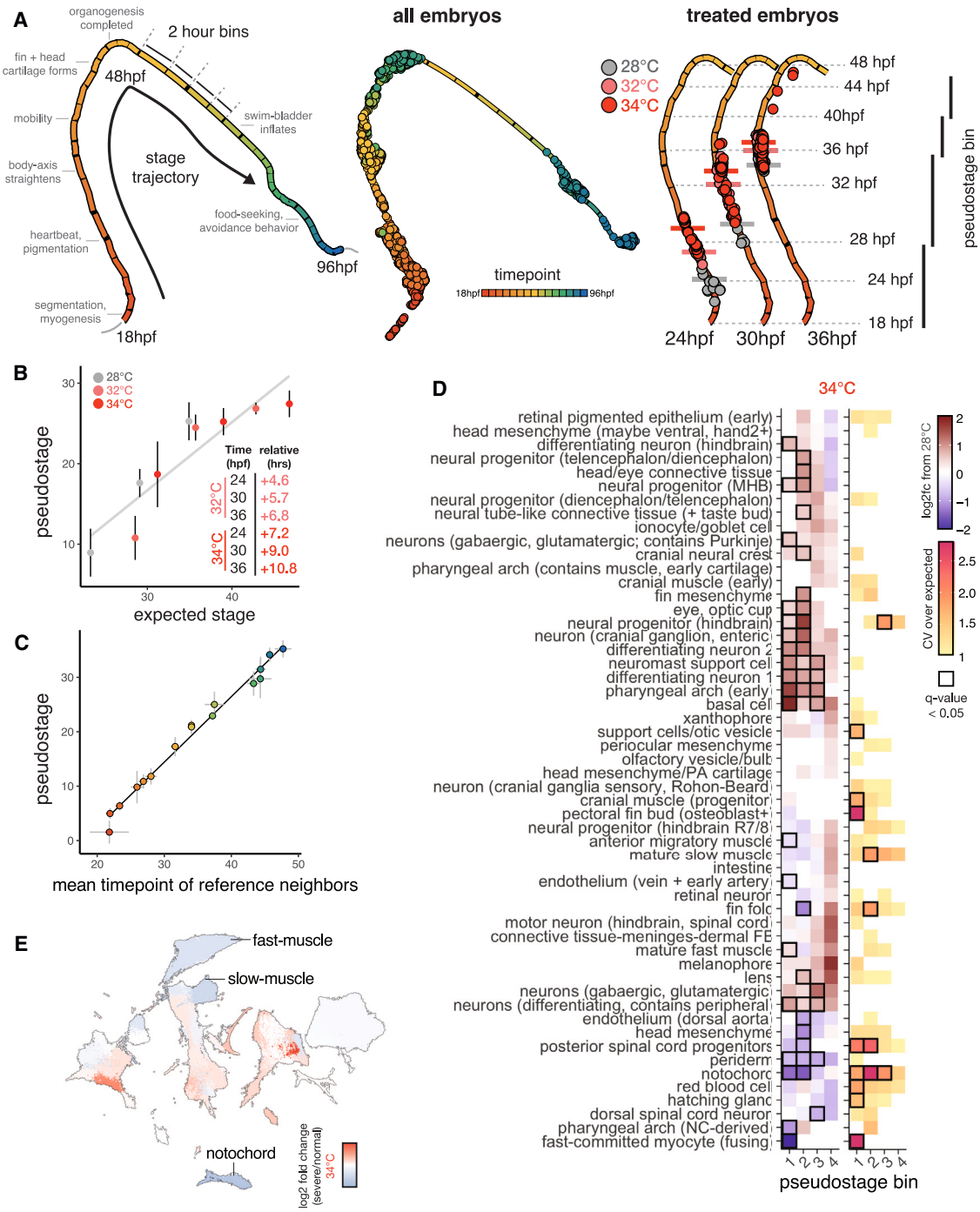

Figure 2. Staging embryos by cell type composition captures temperature-induced acceleration of development and allows isolation of temperature-dependent effects on cell abundance

(A) UMAP of embryo trajectory produced using all individual embryos from the developmental reference; each segment of the principal graph represents a 2-h window of development, with key events noted. Right panel shows how, at each time point, embryos from elevated temperature are "ahead" of their 28°C counterparts on the embryo stage trajectory (median pseduostage for each temperature indicated with horizontal bars).

(B) Scatterplot showing mean pseudostage values are correlated with expectations from a linear model of temperature-induced acceleration of developmental rate; error bars represent standard deviation. The result of linear regression is shown in black.

(C) Scatterplot showing mean pseudostage values for all embryos in the reference dataset compared with a nearest-neighbor label transfer in transcriptome space; error bars on both axes represent standard deviation; both cell composition and transcriptomes contain ample information on developmental stage.

(legend continued on next page)

development despite elevated temperature, all expected cell types were represented in embryos raised at 32°C and 34°C, and we observed no specific activation of heat shock markers hsp90aa1.1 or hsp70L (Figures S1E and S1F) or global activation of the heat shock response (HSR) (Figure S1G), which can diminish cell-type-specific expression patterns.[33]

Variation in developmental stage can be determined from cell type composition

Because of variation in developmental progression over time and temperature, zebrafish studies categorize embryos based on a "staging series" of visible landmarks evident during development at standard temperature. For example, the proper stage-matched control for an embryo raised to 24 hpf at 34°C would be a 31 hpf embryo at 28°C.[24] We therefore sought to develop a method to quantify the degree to which an embryo is accelerated directly from our single-cell data, as staging each embryo is essential for isolating the effects of temperature on cell type composition.

Using our reference dataset (see Saunders et al.[32]), we analyzed individual embryos in two dimensions: embryos were grouped according to similarity in cell type composition, and this grouping produced a trajectory defined primarily by sample time point (Figure 2A, middle, landmarks labeled on left). Individual temperature-treated embryos were projected into this low-dimensional cell composition space and assigned a "pseudostage" value based on their relative position in the trajectory. Because temperature treatment distorts the relationship between clock time and embryo stage, we next tested whether pseudostaging captured the expected increases in developmental rate at high temperature. We projected high-temperature embryos onto the reference embryo cell composition space and found that treated embryos progressed further along the pseudostage trajectory than contemporaneous controls (Figure 2A, right). Pseudostage values were strongly correlated (R^2 = 0.82) to acceleration predicted by a proposed linear model of temperature and developmental stage (Figure 2B; see STAR Methods).[24] We further analyzed individual cell types whose abundance was predictive of whole-embryo pseudostage and found that fin fold cells could be used to precisely stage the embryos (Figures S1H and S1I). Pseudostage values were also strongly correlated with whole-embryo stage values computed from nearest-neighbor average time points in individuals rather than whole-embryo cell type composition (Figure 2C), with the greatest deviation in these metrics appearing at earlier developmental stages (Figure S2A). Thus, whole-embryo cell type composition data captured variation in developmental stage, including that found in untreated embryos sampled at the same clock time (Figure 2B). Staging embryos based on cell type composition was therefore sufficient to control for both biological and technical variation in developmental progression.

Temperature stress alters cell type proportions and injects variability into embryogenesis

Next, we sought to explicitly evaluate the assumption that cell types develop synchronously and in proper proportions in embryos raised at different temperatures. Specifically, we wondered whether we could detect cell-type-specific sensitivity to temperature in cell abundance data, as this may contribute to the stereotyped phenotypes that arise in embryos raised at high temperature. We grouped control and treated embryos of similar developmental stage into four pseudostage bins (Figure 2A, right). Using both absolute cell counts and relative proportions of each cell type per embryo, we performed a regression test using the beta binomial distribution, which is well suited for compositional data.[34,35] After accounting for differences in embryo stage in the model due to the different temperatures, we identified 20–30 cell types that showed significant (q value < 0.05) increases or decreases in abundance with temperature (Figure 2D, left; Table S1A), with a greater number of affected cell types at 34°C than at 32°C. (Figure S2B). Of these, the most strongly affected cell types were notochord, dorsal aorta, and head mesenchyme, showing large reductions in cell number. Among the decreased cell types, there were two groups with physical proximity in the anterior (pharyngeal arch and surrounding head mesenchyme) and posterior (dorsal aorta, posterior spinal cord progenitors, notochord, and fin fold mesenchyme) body. Surprisingly, neural progenitor cell types showed significant increases in abundance, but this was not due to increased signatures of cell-cycle activation at the sampled time points. Other cell types, such as periocular mesenchyme, xanthophore pigment cells, and red blood cells, did not show significant changes in abundance as a function of temperature, suggesting that these cell types are not as sensitive to stress (Figure 2D). The effects of 32°C and 34°C treatments on cell abundances were correlated (R^2 = 0.69), suggesting that these sub-heat shock temperatures affected developmental processes similarly (Figure S2C). Overall, many cell types showed consistent changes in proportion at higher temperatures, even after accounting for developmental stage, reinforcing the notion that stress fundamentally alters cell composition in embryos rather than perturbing development of just a few lineages.

To test whether elevated temperature increased variability in cell composition globally, we compared multinomial models informed by pseudostage alone or by pseudostage and temperature. We found that 42% of the variation in whole-embryo cell composition between 24 and 36 hpf was explained by sample time point, with temperature explaining an additional 12% (Figure S2D), confirming a global increase in anatomical variability. To isolate specific sources of variability during embryogenesis, we identified cell types whose counts showed increased variance over a control expectation (shown as relative coefficient of variation [CV]. After correcting for the dependence of variance on the mean abundance of each cell type, we identified 11 cell

(D) Heatmap showing the effects of temperature on mean cell type abundance relative to untreated, stage-matched controls (left) and on variability (CV relative to controls) of cell counts (right). Significant tests (q < 0.05) from beta binomial regression are indicated with a black box. Each column represents a pseudostage bin, wherein embryos from untreated and treated samples are stage matched.

(E) UMAP of all cell types, colored by relative abundance change in severe (bent) individuals raised at 34°C compared with normal-looking embryos also raised at 34°C.

types showing significant increases in variability at one of the elevated temperatures (Figure 2D, examples in Figure S2E; Table S1B). However, within cell types, the largest dilations in CV occurred in a pseudostage-specific manner (Figure 2D, right). For example, counts of posterior spinal cord progenitors showed increased variability at high temperature in earlier stages but stabilized at later stages (Figure 2D, inset). Across all cell types, on average, relative CV values increased at higher temperatures (Figure S2F) and peaked between pseudostages 20 and 25, consistent with the previous observation that some developmental stages may be more sensitive to stress (Figure S2F, upper panel).[36]

We observed phenotypes of varying severity in embryos raised at high temperatures (severe phenotypes, Figure 1A). We next sought to test whether altered cell composition contributed to differences in phenotypic severity. For embryos raised at 34°C, we classified the phenotype severity for each embryo (Table S2) and, within a single temperature, compared cell type compositions of severe embryos to normal embryos. Embryos with more severe phenotypes showed reduced abundance of several cell types, including notochord, muscle, fin mesenchyme, pharyngeal arch (Figures 2E and S2G), and posterior spinal cord progenitors, suggesting that variation in cell type composition contributes to overall phenotypic variation, even within a temperature. Of these, reduced levels of muscle recruitment in adult zebrafish that experience high temperature during embryonic development[37] have been previously observed, and the body axis defects observed at high temperatures might be expected to affect posterior spinal cord neurons. Profiling cell-type-specific sources of phenotype severity highlights the value of profiling large numbers of replicate embryos. Sensitive detection of temperature-dependent effects on cell abundances would not be possible with just a few replicate embryos, as resultant phenotypes can be obscured by individual-level phenotypic variability.

In summary, we find that some, but not all, cell types show altered abundance as a function of temperature, suggesting that the response to temperature is integrated non-uniformly across cell types. This unexpected result raises the question: what is the molecular basis for these cell-type-specific effects?

Temperature introduces asynchrony in developmental rate across cell types

We next explored whether the temperature-dependent changes in cell type composition were attributable to changes in cell-type-specific developmental rates. While the embryo as a whole develops 4–6 h more quickly when raised at 32°C/34°C than at the standard 28°C (Figure 2B, inset), variation in this acceleration across cell types has not previously been measured. To determine whether cell-type-specific developmental rates vary, we examined relative differences in each cell type's transcriptional "age," a measure derived from comparison to our developmental reference, in temperature treatments compared with controls (Figure S3A; see STAR Methods). Taking the mean age of all cells for each embryo captures whole-embryo acceleration similar to the pseudostage metric (Figure S3B). For example, notochord cells in embryos raised at 32°C and 34°C showed +1.6 h and +2.2 h acceleration of transcriptional age relative to the whole-embryo expectation (Figure S3C). Several additional cell types, including the dorsal aorta, melanophore, and hypochord cells (Figure 3A, middle), showed a similar relative advancement, and we classified these cells as highly accelerated (Figure 3B). In contrast, basal cells, pigment progenitors, and fin fold cells were unresponsive or decelerated at high temperature (Figure S3C). To ensure that this signal of developmental acceleration was indeed driven by core genes related to progression of each cell type rather than a subset of temperature-responsive genes, we analyzed the number of differentially expressed genes associated with temperature after accounting for developmental stage. For most cell types (85%), the number of significantly differentially expressed genes associated with developmental stage is greater than the number associated with temperature, highlighting the importance of including developmental-stage information to properly isolate the effects of an environmental perturbation from effects on developmental delay or acceleration (Figure S3D). Furthermore, developmental acceleration is associated with changes across the transcriptome rather than being concentrated in a small number of sensitive genes. In the notochord, which showed strong temperature-dependent acceleration, we found no apparent relationship between genes differentially expressed at high temperature and those changing significantly with developmental age, but temperature-induced genes tended to be more highly expressed than those associated with developmental age (Figures S5E and S5F).

Given that some cell types were more developmentally accelerated than others, we next sought to directly quantify the synchrony of development across cell types. We first assessed variation in developmental stage at the embryo level by examining pseudostage deviations at each temperature; both temperatures increased variability in developmental stage (Figure 3E). We also found that coordinated developmental timing between cell types could be observed in the covariance structure of cell type ages across all embryos (Figure 3F). As expected, there was a positive correlation in age between all cell type pairs in control embryos (average $r = 0.24$) (Figure 3G). However, we found that the covariance structure between cell types was disrupted in both of our elevated temperature conditions; the correlation of transcriptional age between cell type pairs was reduced by 3-fold on average (Figure 3G). Furthermore, many cell type pairs that showed coordinated activation of cell-cycle-related genes also showed reduced correlation in elevated temperature conditions, suggesting loss of coordinated growth (Figure S3G). Together, these results highlight how temperature introduces a non-uniform increase in developmental rate across different cell types and disrupts the developmental synchrony between cell types. Together, these results highlight an additional source of temperature-induced variability during development: asynchrony in developmental rate emerging from cell-type-specific sensitivity to temperature.

Without an obvious anatomical or lineal relationship uniting highly accelerated cell types, we wondered whether any underlying molecular processes could explain differential developmental acceleration. Differences in developmental rate under temperature stress and between species have been variously associated with metabolic rate, cell division, protein degradation, and protein

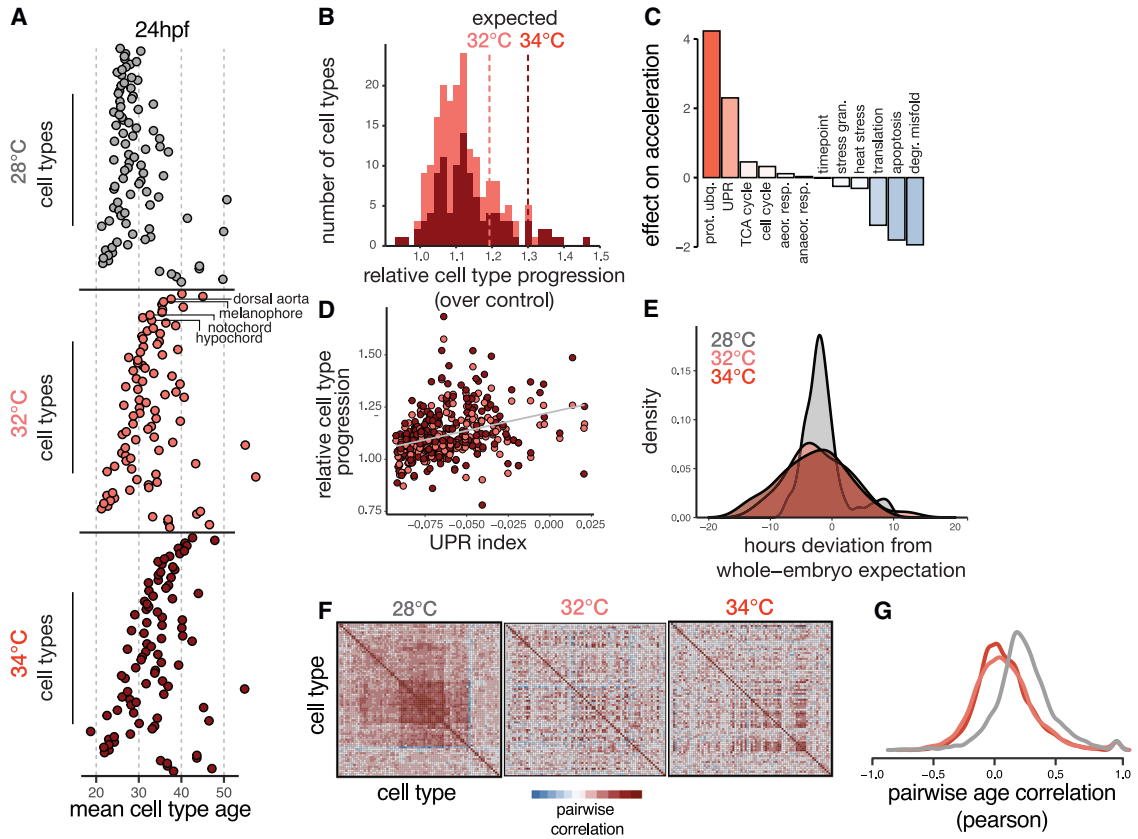

Figure 3. Temperature introduces asynchrony in developmental rate across cell types

(A) Dot plots showing the transcriptional ages of all cell types at 24 hpf, faceted by temperature. Cell types on the y axis are ordered by their relative acceleration at 34°C, highlighting the most sensitive cell types near the top and insensitive types near the bottom. Cell type ordering is the same for all temperatures; specific examples are indicated with labels.

(B) Histogram showing distributions of relative cell type progression at each temperature, with vertical lines showing the relative progression expected for the whole embryo.

(C) Bar plot showing the effect sizes for expression levels of several cellular processes related to metabolism, protein folding, proliferation, and stress response in an additive model predicting relative progression of the cell type at high temperature.

(D) Scatterplot showing basal levels of the UPR in each cell type against its relative progression, revealing a positive trend for both temperatures.

(E) Density histogram showing increased variance in developmental stage for embryos raised at elevated temperature.

(F) Heatmaps showing pairwise correlation coefficients of transcriptional age for all cell types in the embryo; at 28°C, most cell type pairs are positively correlated across individual embryos, whereas this correlation structure is diminished at elevated temperatures.

(G) Density histogram of pairwise correlation values at each temperature, summarizing the loss in correlation structure seen in (F).

synthesis.[5,6,38] Accordingly, we generated signature scores for these processes, as well as two stress pathways, the UPR and the HSR, to identify those with the strongest effect in predicting relative acceleration of cell-type-specific developmental rate. To test this, we modeled the developmental rate increases across cell types as a function of baseline (during normal development at standard temperature) expression of genes important for each process (Figure 3C, inset). We verified that neither the basal nor induced HSR was strongly correlated with temperature-dependent acceleration, consistent with a temperature treatment that challenges proteostasis but does not activate a canonical HSR (Figures S1E–S1G, S3H, and S3I). Cell types expressing higher levels of genes involved in protein synthesis, apoptosis, and degradation of misfolded protein showed less temperature-dependent acceleration of development (Figure 3C), slowing down relative to whole-embryo expectation. We validated the effect of protein synthesis on slowing developmental rate by treating embryos with low-dose cyclohexamide (CHX) and 20°C cold treatment; delayed progression was evident in both treatments (Figures S4A and S4B). Furthermore, the effects of protein synthesis inhibition on gene expression were strongly correlated with effects of cold treatment (Figures S4C and S4D). Lastly, we identified genes with opposing transcriptional responses to both 20°C and 34°C treatment, including translation elongation factor eef2b in muscle cells (Figures S4E and S4F), suggesting that control of protein levels may contribute to cell-type-specific temperature response. Cell types with high expression of genes involved in protein ubiquitination and the UPR showed more temperature-dependent acceleration of development than those with lower expression of these processes. That temperature-dependent acceleration across all cell types could be partially explained by baseline levels of UPR suggests a role for endoplasmic reticulum

(ER) stress in modulating developmental rate under normal conditions (Figure 3D). Activation of UPR during normal development has been observed in both the notochord and the hatching gland[39–42] in fish, as well as during cell differentiation and growth in other models,[43,44] but has not been previously linked to developmental rate.

The UPR buffers notochord-specific temperature sensitivity

To explore whether transcriptional responses to temperature, similar to changes in cell abundances and developmental age, were non-uniform across cell types, we analyzed genes with differential expression at higher temperatures. We identified several modules of genes that tended to be upregulated in response to elevated temperature (Figure S5A; Table S3A). These modules were enriched for genes related to cell cycle, chromatin organization, transcription, ion transport, and protein processing in the ER, but not the canonical HSR (Figure S5A; Table S3B). In contrast to global activation of the HSR,[33] these temperature-responsive modules tended to be upregulated in a cell-type-specific manner (Figure S5B). For example, only blood cells showed activation of the cell-cycle module, while the notochord showed concomitant activation of translation and ER stress modules (Figure S5B, boxed). Of all the temperature-response modules, the ER stress gene cluster showed the broadest response across tissues.

The unexpected appearance of the UPR (Figure 3C) and a gene module for translation and ER stress (Figure S5A) among cell-type-specific responses to temperature led us to explore this phenomenon more deeply across cell types. We generated signature scores for translation and the UPR in all cell types in individual embryos and found that cells tended to express high levels of either one signature or the other, consistent with the UPR's role in attenuating translation (Figure 4A; Table S3C).[45] In contrast, we observed in the notochord a simultaneous upregulation of UPR and translation that are specific to elevated temperature conditions (Figures 4B and S5C). This exceptional upregulation of translation in the presence of UPR is pronounced to a lesser extent in the hypochord and pectoral fin bud; nearly all other cell types showed reductions in the number of cells expressing both signatures (Figure 4B). Notably, the notochord showed temperature-dependent effects on cell abundance as well as a marked acceleration of developmental age (Figures 2E, 3A, and S5D). We wondered whether this exceptional upregulation of UPR and translation might be related to the notochord's apparent sensitivity to temperature.

The notochord has unique mechanical and signaling functions, with specific cell subtypes carrying out these roles. These notochord subtypes are apparent in the reference dataset, including the vacuolated inner cells (*rab32a*$^{+}$, *cav3*$^{+}$), epithelial-like sheath cells (*col8a1*$^{+}$), and pre-mineralization sheath cells (*entpd5a*$^{+}$) (Figure 4C), with these subtypes diverging earlier in development (Figure 4D). To identify which of these types might be responsible for its temperature sensitivity, we compared notochord cells from embryos raised in elevated temperatures with notochord cells from our wild-type reference dataset (Figure 4E). We detected significant ($q < 0.05$) enrichment for cells from the elevated temperature condition in focal regions of the notochord UMAP, including a "hotspot" among the epithelial-like sheath cells, which expressed genes for translation and UPR at higher levels than other notochord subtypes (Figure 5A). The primary functions of the epithelial-like sheath cells are to produce, process, and package large amounts of collagen and extracellular matrix proteins that will ultimately be secreted to produce the extracellular notochord sheath, which is essential for the rigidity of the notochord and the proper formation of the embryonic body.[46]

To test whether UPR buffers temperature-mediated ER stress in the developing notochord, we used CRISPR in F0 embryos to knock out the ER stress-sensing transcription factor Atf6 and examined notochord morphology using Alcian blue stain. In accordance with previous descriptions in medaka fish,[41] we observed slight notochord defects at both 24 hpf and 48 hpf when fish were raised at standard temperature (Figure 5A), and nearly all *atf6* crispants were viable past 24 hpf. We next tested whether defects in *atf6* crispants were exacerbated when these embryos were raised at elevated temperature, especially given the proteostatic stress expected from temperature-dependent upregulation of translation in the notochord. Notochords from control fish raised at elevated temperature looked normal except for the usual bends, while *atf6* crispant fish showed kinks, bends, or deformations of the notochord sheath (Figure 5A). These phenotypes evoke notochord mutants that affect the structural integrity of the sheath, such as *col8a1*, rather than the mutants affecting vacuolation, such as *rab32a*.[47,48]

To further test how the role of Atf6 in activating UPR in the notochord affects its ability to withstand temperature stress, we performed an additional sci-Plex experiment on 96 individual embryos of *atf6* crispants and injection controls raised at normal and high temperature. We found that both whole-embryo and notochord-specific developmental age was lower than expected when *atf6* crispant embryos were raised at high temperature (Figure 5B). Additionally, pharmacological inhibition of UPR with integrated stress response inhibitor (ISRIB) in embryos raised at high temperature prevented notochord sheath cells from entering the stress-induced hotspot transcriptional state (Figure 4D), though temperature-induced developmental acceleration was still apparent at 48 hpf with this treatment, suggesting some functional separation between components of the UPR in control of acceleration (Figures S5E and S5F). While *atf6* crispants showed reduced temperature-dependent acceleration of development, both notochord-specific and embryo-wide developmental ages were unaffected when mutants were raised at the normal temperature (Figure 5B). Therefore, *atf6* crispants did not show generalized developmental delay but rather a deficiency in accelerating development in response to increased temperature. This result was consistent with our finding that basal UPR levels in each cell type were correlated with temperature-dependent acceleration of their development (Figure 3C), highlighting the role of the UPR in coordinating cell-type-specific changes of developmental timing in the embryo. Based on the requirement of UPR for temperature-accelerated development in individual cell types, we next sought to understand cell-type-specific consequences of impaired control of timing and phenotypic severity of *atf6* crispants.

Because the sheath cells showed a potent upregulation of genes required for translation in response to increased

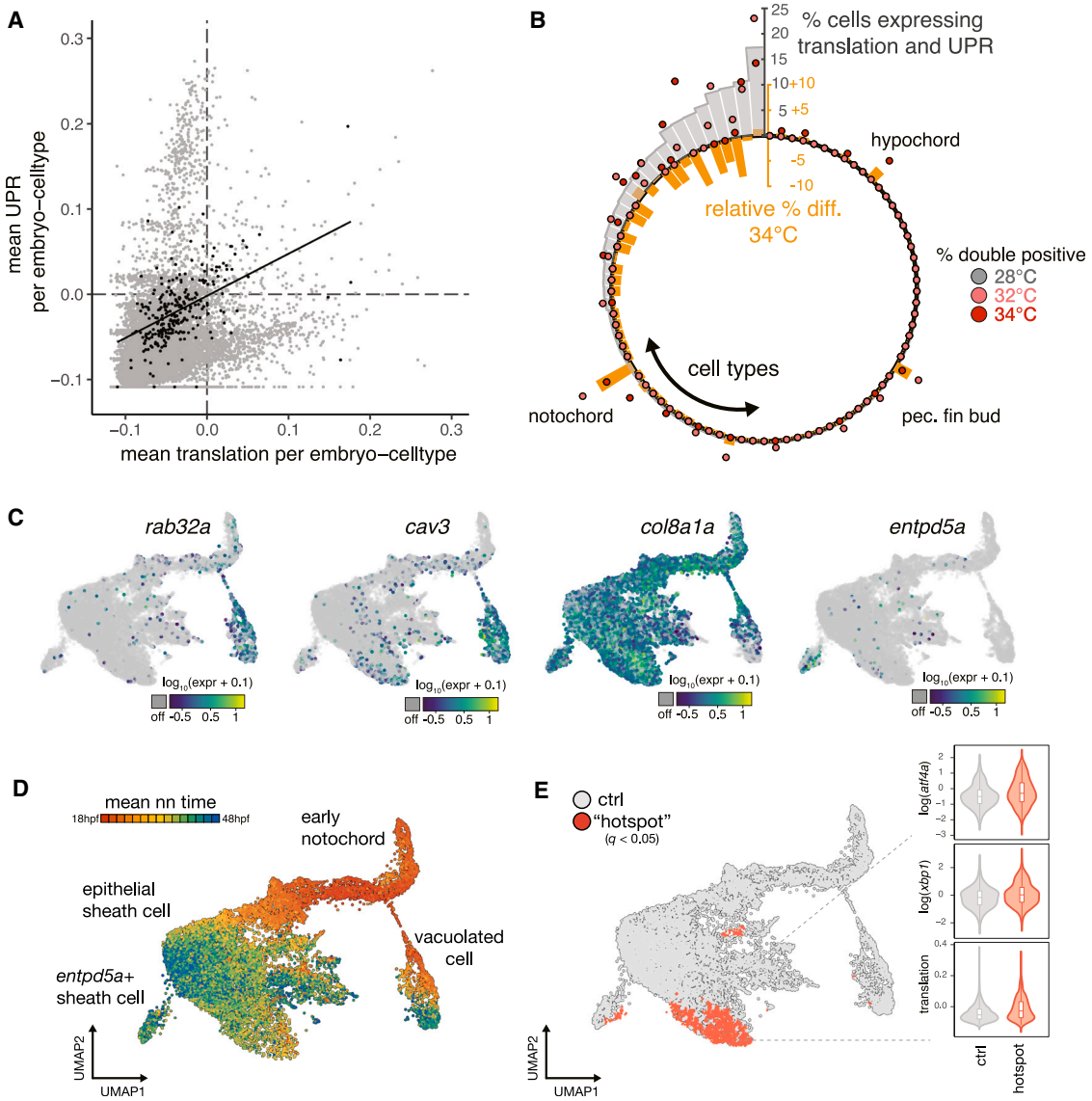

Figure 4. Exceptional regulation of the UPR underlies temperature sensitivity in the notochord

(A) Scatterplot showing levels of translation signature and UPR signature across all embryo cell types. Consistent with known translational attenuation by UPR, these processes are generally uncorrelated across cell types. The notochord (plotted as black dots) is an exception, with a positive correlation (Pearson's r = 0.51) between these processes and appreciable levels of both UPR and translation in a subset of embryos.

(B) Circular bar plot showing occurrence of translation + UPR co-expression, displayed as percentage of double positive in each cell type (gray bars). Overlaid dots show raw percentage of double-positive cells for embryos raised at elevated temperature, colored pink and dark red for 32°C and 34°C, respectively. Orange bars show the relative change in the fraction of double-positive cells in each cell type at elevated temperatures. For the large majority of cell types, this difference is negative. The notochord, hypochord, and pectoral fin bud are the sole exceptions, where double-positive cells increase in response to temperature increase.

(C) Marker gene plots showing expression of genes defining notochord subtypes (*rab32a* and *cav3* in vacuolated cells; *col8a1a* in sheath cells; *entpd5a* in pre-mineralization sheath cells).

(D) UMAP showing co-embedded notochord cells from reference and temperature perturbation experiment, colored according to the mean time point label of nearest neighbors in the reference. Annotations for each cell type are indicated.

(E) UMAP showing sheath cells from temperature perturbation experiment with significant spatial bias using hotspot test ($q < 0.05$) in UMAP space (see STAR Methods). Cells with a significant spatial base are shown in red. Inset shows levels of UPR markers and translation signature in these cells increasing with temperature.

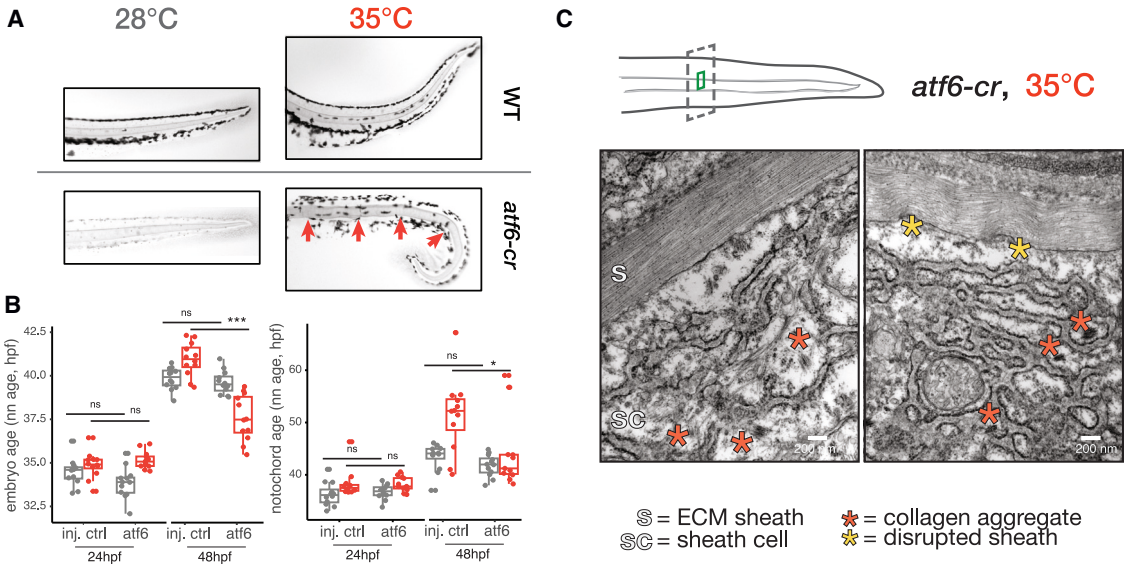

Figure 5. Loss of Atf6 limits temperature-induced acceleration of developmental rate and increases temperature sensitivity of the notochord

(A) Images of Alcian blue-stained notochords (camera image in black and white) in the tails of wild-type and *atf6* crispant embryos raised at 28°C and 35°C. Examples of notochord defects in crispants raised at elevated temperature, kinks indicated with red arrows (phenylthiourea was used for imaging 28°C crispants).

(B) Box plots showing reduced capacity for acceleration of development at 34°C for the entire embryo (left) and notochord (right), while no developmental delay is apparent at 28°C.

(C) Results of TEM of notochord sheath cells in *atf6* crispants raised at elevated temperature, showing disrupted ER structure and aggregated collagen fibrils (red asterisks). Scale bar, 200 nm; sc, sheath cell; s, sheath.

temperature (Figure 5A), we wondered whether this cell type was functioning properly in deposition of the notochord sheath. We examined the ultrastructure of sheath cells and the sheath using transmission electron microscopy (TEM). We confirmed that the notochord sheath showed increased disorder at 35°C in both wild-type and *atf6* crispant fish compared with controls raised at standard temperature (Figure 5C, see comparison in Figure S5G), suggesting that proper modification and organization of collagen is challenged at elevated temperature. Furthermore, we noted a dense, altered ER structure in this condition (Figure S5G). The most striking difference in *atf6* mutants raised at high temperature was an accumulation of misfolded, non-secreted collagen fibers in the sheath cells themselves (Figure 5B). Both protein aggregates and the severe disruption of ER structure in these fish suggested a failure of export, likely owing to the increased burden of protein synthesis at high temperatures combined with a lack of a properly functioning ER stress response. Taken together, these experiments showed that in order for the notochord to structurally support the developing embryo, one of its cell types must operate near its proteostatic limits, requiring management by the UPR even at normal temperatures. Elevated temperature pushed the notochord sheath cells past their proteostatic limits, leading to protein aggregation, cellular defects, and a compromised notochord sheath that ultimately leads to a bent tail.

DISCUSSION

Here, we used large-scale single-cell profiling of individual zebrafish embryos to explore how water temperature impacted their development. To do so, we introduced novel computational approaches to detect and isolate the effects of temperature on the abundance and transcriptomes of all cell types.

In characterizing cell-type-specific responses to temperature in embryos, we identified previously overlooked sources of compromised developmental robustness. First, we found variability in the temperature-induced developmental acceleration across cell types, introducing asynchrony in the coordinated and timely traversal of developmental trajectories. This phenomenon was not unlike the consequence of genetic mutants causing stalling or mis-timed events of single cell types in the coordinated program of development.[49] Unlike in these genetic mutants, elevated temperature did not induce stalling in any single cell type but rather introduced asynchrony across cell types; the degree of accelerations among cell types ranged from negligible to over 40%, and correlated progression between cell types was lost. This loss of synchrony between cell types that signal to one another during embryonic development may have broad consequences for tissue morphogenesis and may be related to documented non-cell-autonomous effects of cell-type-specific temperature sensing.[50,51] Further efforts to examine pairs of cell types with known signaling interactions may explain the observed patterns of synchrony loss. In sum, elevated temperature challenged the robustness of the developmental program by introducing non-uniform acceleration of developmental timing across cell types, breaking synchrony across the embryo.

What mechanisms could allow for this critical vulnerability in development? All cells have the capacity to sense and respond to temperature. The classic example is heat shock, a threshold

phenomenon wherein cells experiencing an upward shift in temperature rapidly activate a suite of heat shock proteins to manage the acute stress. The temperatures we used in this study did not meet this threshold, and, accordingly, we observed no activation of the canonical HSR (Figures S1D–S1F). Even so, the developmental rate of the embryos showed a continuous, linear relationship with temperature in the 25°C–35°C range,[24] revealing the existence of a temperature-sensitive gene program outside of the HSR linked to control of timing. Surprisingly, we found that the relationship between temperature and developmental rate was non-uniform at the level of cell type, with some cell types accelerating more than others in response to the same elevated temperature. Therefore, distinct cell types appeared to be differentially sensitive to temperature.

We used two additional treatments to push developmental rate in the opposite direction: cooler temperatures and a non-lethal dose of the protein synthesis inhibitor CHX. In comparing these treatments, we detected effects of each perturbation on global gene expression even within embryos at the same developmental stage. We found that the majority of gene expression differences found in both of these delay-inducing treatments were the same genes affected during warm temperature treatment but with the opposite sign (see Figures S4E and S4F), suggesting a common sensing mechanism to adjust developmental rate.

Cell-type-specific sensitivity to temperature was also evident in the altered cell composition of embryos raised under stress. Whether the cellular phenotypes displayed by embryos raised at high temperature were of any adaptive value was unclear. Further study of natural populations and related species will be required to further explore this question, because lab populations of zebrafish show reduced plasticity and thermal tolerance relative to their wild counterparts.[52] The notochord was especially sensitive, owing to the burden of protein synthesis in epithelial sheath cells, which, under high-temperature conditions, accumulate misfolded protein. The developing notochord depended on high levels of protein synthesis,[53] ER chaperone function,[54] and specialized secretion[42] to construct a well-ordered, collagen-rich sheath. This resulted in considerable stress on the ER and physiological activation of the UPR. The surprising upregulation of translation in these cells despite presumed translational attenuation by the UPR suggested that sheath cells might bypass translation regulation to achieve their exceptional protein synthesis capacity.[55] Several other cell types with high demands of protein expression also depended on stress responses during normal development; the UPR was activated in the hatching gland, periderm, and vascular smooth muscle and via the HSR, and cytoplasmic chaperones were activated in red blood cells, fast muscle, and cardiomyocytes. While the consequences of excessive burden on protein homeostasis in cells are evident in the aggregation associated with neurodegenerative diseases,[56] we noted the impact of this burden during embryogenesis, when even a transient stress may irreversibly perturb normal development. Furthermore, while basal activation of homeostatic mechanisms such as the UPR bestowed some cell types (like the notochord) with additional capacity for pushing the limits of proteostasis during normal development, they necessarily brought along additional risk: the evolution of developmental programs that overdraw on the essential stress response mechanisms required to deal with unexpected environmental changes. As with the HSR, the UPR showed deep evolutionary conservation in managing proteostatic stress, but the additional challenges of multicellularity may have driven these stress-associated pathways toward new functions. Indeed, the UPR pathway showed increasingly elaborate control through evolutionary time, such as the capacity for protein synthesis control in the transition from unicellular to multicellular eukaryotes.[57]

Proteostasis is maintained throughout different cell types and stages of development but can be broken under environmental stress. The consequences of this breakdown are borne unevenly across cell types, each according to their respective demands on the pathways required to maintain homeostasis. Despite these heterogeneous demands on proteostasis control, how is a uniform acceleration of all cell types coordinated to achieve more rapid development at increased temperature? First, we have shown that this acceleration is not uniform; significant variability in acceleration is apparent at higher temperatures, and synchrony among cell types is reduced (Figures 3E–3G). Even so, temperature has a predictable mean effect on acceleration[24] and also pushes most cell types forward along their differentiation trajectories, suggesting some level of global control. We propose that this global control arises at least in part through management of proteostasis by the UPR; cell types with higher basal activation of UPR show greater temperature-induced acceleration (Figure 3B), and UPR is required for temperature-induced acceleration (Figure 5B). While the precise mechanism is not yet clear, UPR-dependent control of developmental timing may arise from a cell-autonomous phenomenon in all cell types (such as control of protein synthesis levels) or from a non-cell-autonomous coordination via a subset of sensitive cell types (such as the notochord) with the ability to influence developmental rate of surrounding cells. These two mechanisms are not mutually exclusive, but further experiments will be required to directly test the requirement for non-autonomous control of synchrony in temperature-induced acceleration. Furthermore, the UPR may converge on other aspects of the broader environmental stress response (ESR) to help synchronize cells during development; further genetic experiments may clarify which of the many sensors and signal transduction components of the ESR contribute to its control as well as the relative importance of chromatin organization, transcriptional and translational control, and other cellular processes. Our study provides a methodological path forward for such studies.

We propose that cell types with high demands on proteostasis during normal development may be more susceptible to further perturbations of homeostasis by temperature or other environmental stressors. Further exploration into the differential demands placed on each cell type by ancient and general molecular processes may shed new light on how stress on a molecular pathway in a specific cell type generates phenotypes at the tissue, organ, or organismal scale.

Limitations of the study

The technology presented in this study allows for theoretically limitless sample multiplexing, opening up analysis of biological

replicate embryos. However, this approach depends on nuclear rather than whole-cell single-cell RNA-seq data, and while this kind of data produces less-biased cellular sampling of the embryo, it brings limitations in the total number of RNA molecules captured per cell. Further improvements to mRNA capture efficiency in this protocol would add statistical power in identifying more subtle gene expression differences induced by temperature stress.

Our study shows that zebrafish embryos raised at elevated temperature have altered cell type composition and differential gene expression at important junctures of organogenesis. While the high time resolution and cellular coverage of many biological replicate embryos from the commonly studied AB strain indeed supports this finding, the adaptive relevance in wild zebrafish remains to be ascertained. Warming water systems create an urgent need for further studies in natural populations and related species to explore this question. Lab populations of zebrafish do show reduced plasticity and thermal tolerance relative to their wild counterparts[52] and may therefore be less resilient when developing in warm water, but both the cellular mechanisms and cell types central to temperature-dependent developmental acceleration are highly conserved across vertebrates. The changes we observed are therefore likely to be broadly relevant. Supported by imaging data, we find that the reduced abundance of notochord cells is associated with failure of sheath cell function at high temperature, but we have not quantitatively assessed the nature of other cell abundance changes we observed. Why do some cell types increase in abundance relative to untreated embryos? Follow-up studies will be required to link these cell type composition changes to whole-embryo or persistent adult phenotypes. Further, the groups of cell types with affected abundance may reflect underlying cell-cell signaling interactions. Individual embryo data open many opportunities to infer how cell types interact with each other, but identifying these interactions is a nontrivial statistical problem.

Finally, our model of developmental robustness implies that building an embryo of correct proportions depends on precise timing and coordination among developmental trajectories of different cell types. We have shown that this timing and coordination is achieved, in part, through control of cellular proteostasis via the UPR. However, beyond direct visualization of large proteins in the notochord sheath, we have not been able to directly connect a protein-level measurement with our single-cell analysis of developmental trajectories throughout the embryo. To fully realize this goal would require technical advances in single-cell proteomic tools. The ability to track protein levels, or of protein synthesis activity, in many cell types through developmental time and in response to temperature would permit a general test of our model.

STAR★METHODS

Detailed methods are provided in the online version of this paper and include the following:

- KEY RESOURCES TABLE
- RESOURCE AVAILABILITY
  - Lead contact
  - Materials availability
  - Data and code availability
- EXPERIMENTAL MODEL AND STUDY PARTICIPANT DETAILS
  - Animals
- METHOD DETAILS
  - Preparation of barcoded nuclei from individual embryos
  - Sci-RNA-seq3 library construction
  - Sequencing, read processing and cell filtering
  - Count matrix pre-processing
  - Cell annotation by projection of query data to reference
  - Estimation of transcriptional age for each cell and cell type
  - Comparison of embryo pseudostage with conventional staging
  - Additive model for cell-type-specific acceleration
  - Perturbation of proteostasis via CRISPR-Cas9 mutagenesis and inhibitors
  - Transmission electron microscopy
  - Notochord staining
  - Differential gene expression analysis
  - Hotspot analysis
- QUANTIFICATION AND STATISTICAL ANALYSIS
  - Cell abundance and variance statistics
- ADDITIONAL RESOURCES

SUPPLEMENTAL INFORMATION

Supplemental information can be found online at https://doi.org/10.1016/j.cell.2023.10.013.

ACKNOWLEDGMENTS

We thank Nola Klemfuss and the Brotman Baty Institute Advanced Technology Lab for support with sequencing and data processing. We also thank Frank Steemers and Fan Zhang for additional sequencing support. We thank Ed Parker for assistance with TEM. This work was supported by a grant from the Paul G. Allen Frontiers Group (Allen Discovery Center for Cell Lineage Tracing to C.T. and J.S.) and the National Institutes of Health (UM1HG011586 to C.T. and J.S.; 1R01HG010632 to C.T. and J.S.). J.S. is an investigator of the Howard Hughes Medical Institute. M.W.D. was supported by UM1HG011586 to C.T. and NHGRI 1RM1HG010461 to C.Q.

AUTHOR CONTRIBUTIONS

M.W.D., L.M.S., and C.T. designed the study. M.W.D., L.M.S., and S.S. performed sci-RNA-seq3 experiments. M.W.D. performed computational analyses with M.D., B.E., and C.T. D.K. performed notochord staining. M.W.D. and C.T. wrote the manuscript with input from all coauthors. J.S., C.Q., D.R., and D.K. contributed methods, supervision, and edited the manuscript. C.T. supervised the project.

DECLARATION OF INTERESTS

C.T. is a scientific advisory board (SAB) member, consultant, and/or co-founder of Algen Biotechnologies, Altius Therapeutics, and Scale Biosciences. J.S. is an SAB member, consultant, and/or co-founder of Cajal Neuroscience, Guardant Health, Maze Therapeutics, Camp4 Therapeutics, Phase Genomics, Adaptive Biotechnologies, and Scale Biosciences.

Received: September 22, 2022
Revised: May 29, 2023
Accepted: October 11, 2023
Published: November 9, 2023

REFERENCES

1. Schirone, R.C., and Gross, L. (1968). Effect of temperature on early embryological development of the zebra fish, Brachydanio rerio. J. Exp. Zool. *169*, 43–52.
2. Sharpe, P.J., and DeMichele, D.W. (1977). Reaction kinetics of poikilotherm development. J. Theor. Biol. *64*, 649–670.
3. Kuntz, S.G., and Eisen, M.B. (2014). Drosophila embryogenesis scales uniformly across temperature in developmentally diverse species. PLoS Genet. *10*, e1004293.
4. Gillooly, J.F., Charnov, E.L., West, G.B., Savage, V.M., and Brown, J.H. (2002). Effects of size and temperature on developmental time. Nature *417*, 70–73.
5. Rayon, T., Stamataki, D., Perez-Carrasco, R., Garcia-Perez, L., Barrington, C., Melchionda, M., Exelby, K., Lazaro, J., Tybulewicz, V.L.J., Fisher, E.M.C., and Briscoe, J. (2020). Species-specific pace of development is associated with differences in protein stability. Science *369*, eaba7667. https://doi.org/10.1126/science.aba7667.
6. Matsuda, M., Hayashi, H., Garcia-Ojalvo, J., Yoshioka-Kobayashi, K., Kageyama, R., Yamanaka, Y., Ikeya, M., Toguchida, J., Alev, C., and Ebisuya, M. (2020). Species-specific segmentation clock periods are due to differential biochemical reaction speeds. Science *369*, 1450–1455.
7. Min, M., Rong, Y., Tian, C., and Spencer, S.L. (2020). Temporal integration of mitogen history in mother cells controls proliferation of daughter cells. Science *368*, 1261–1265.
8. Jarosz, D.F., Taipale, M., and Lindquist, S. (2010). Protein homeostasis and the phenotypic manifestation of genetic diversity: principles and mechanisms. Annu. Rev. Genet. *44*, 189–216.
9. Balchin, D., Hayer-Hartl, M., and Hartl, F.U. (2016). In vivo aspects of protein folding and quality control. Science *353*, aac4354.
10. Queitsch, C., Sangster, T.A., and Lindquist, S. (2002). Hsp90 as a capacitor of phenotypic variation. Nature *417*, 618–624.
11. Jarosz, D.F., and Lindquist, S. (2010). Hsp90 and environmental stress transform the adaptive value of natural genetic variation. Science *330*, 1820–1824.
12. Rohner, N., Jarosz, D.F., Kowalko, J.E., Yoshizawa, M., Jeffery, W.R., Borowsky, R.L., Lindquist, S., and Tabin, C.J. (2013). Cryptic variation in morphological evolution: HSP90 as a capacitor for loss of eyes in cavefish. Science *342*, 1372–1375.
13. Rutherford, S.L., and Lindquist, S. (1998). Hsp90 as a capacitor for morphological evolution. Nature *396*, 336–342.
14. Isaacs, W.B., and Fulton, A.B. (1987). Cotranslational assembly of myosin heavy chain in developing cultured skeletal muscle. Proc. Natl. Acad. Sci. USA *84*, 6174–6178.
15. Hetz, C. (2021). Adapting the proteostasis capacity to sustain brain healthspan. Cell *184*, 1545–1560. https://doi.org/10.1016/j.cell.2021.02.007.
16. Rutherford, S.L. (2003). Between genotype and phenotype: protein chaperones and evolvability. Nat. Rev. Genet. *4*, 263–274.
17. Goldschmidt, R. (1929). Experimentelle Mutation und das Problem der sogenannten Parallelinduktion Versuche an Drosophila. Biologischen Zentralblatt *49*, 437–448.
18. Audzijonyte, A., Richards, S.A., Stuart-Smith, R.D., Pecl, G., Edgar, G.J., Barrett, N.S., Payne, N., and Blanchard, J.L. (2020). Fish body sizes change with temperature but not all species shrink with warming. Nat. Ecol. Evol. *4*, 809–814.
19. Hsu, C.-Y., and Chiu, Y.-C. (2009). Ambient temperature influences aging in an annual fish (Nothobranchius rachovii). Aging Cell *8*, 726–737.
20. Engeszer, R.E., Patterson, L.B., Rao, A.A., and Parichy, D.M. (2007). Zebrafish in the wild: a review of natural history and new notes from the field. Zebrafish *4*, 21–40.
21. Cockroft, D.L., and New, D.A. (1978). Abnormalities induced in cultured rat embryos by hyperthermia. Teratology *17*, 277–283.
22. Germain, M.A., Webster, W.S., and Edwards, M.J. (1985). Hyperthermia as a teratogen: parameters determining hyperthermia-induced head defects in the rat. Teratology *31*, 265–272.
23. Shoji, W., and Sato-Maeda, M. (2008). Application of heat shock promoter in transgenic zebrafish. Dev. Growth Differ. *50*, 401–406.
24. Kimmel, C.B., Ballard, W.W., Kimmel, S.R., Ullmann, B., and Schilling, T.F. (1995). Stages of embryonic development of the zebrafish. Dev. Dyn. *203*, 253–310.
25. Schmidt, K., and Starck, J.M. (2010). Developmental plasticity, modularity, and heterochrony during the phylotypic stage of the zebra fish, Danio rerio. J. Exp. Zool. B Mol. Dev. Evol. *314*, 166–178.
26. Sfakianakis, D.G., Leris, I., and Kentouri, M. (2012). Exercise–related muscle lactate metabolism in zebrafish juveniles: The effect of early life temperature. Ital. J. Zool. *79*, 568–573.
27. Ackerly, K.L., and Ward, A.B. (2016). How temperature-induced variation in musculoskeletal anatomy affects escape performance and survival of zebrafish (Danio rerio). J. Exp. Zool. A Ecol. Genet. Physiol. *325*, 25–40.
28. Srivatsan, S.R., McFaline-Figueroa, J.L., Ramani, V., Saunders, L., Cao, J., Packer, J., Pliner, H.A., Jackson, D.L., Daza, R.M., Christiansen, L., et al. (2020). Massively multiplex chemical transcriptomics at single-cell resolution. Science *367*, 45–51.
29. Cao, J., Spielmann, M., Qiu, X., Huang, X., Ibrahim, D.M., Hill, A.J., Zhang, F., Mundlos, S., Christiansen, L., Steemers, F.J., et al. (2019). The single-cell transcriptional landscape of mammalian organogenesis. Nature *566*, 496–502.
30. Wagner, D.E., Weinreb, C., Collins, Z.M., Briggs, J.A., Megason, S.G., and Klein, A.M. (2018). Single-cell mapping of gene expression landscapes and lineage in the zebrafish embryo. Science *360*, 981–987.
31. Farnsworth, D.R., Posner, M., and Miller, A.C. (2021). Single cell transcriptomics of the developing zebrafish lens and identification of putative controllers of lens development. Exp. Eye Res. *206*, 108535.
32. Saunders, L.M., Srivatsan, S.R., Duran, M., Dorrity, M.W., Ewing, B., Linbo, T., Shendure, J., Raible, D.W., Moens, C.B., Kimelman, D., et al. (2023). Embryo-scale reverse genetics at single-cell resolution. Nature.. https://doi.org/10.1038/s41586-023-06720-2.
33. Jean-Baptiste, K., McFaline-Figueroa, J.L., Alexandre, C.M., Dorrity, M.W., Saunders, L., Bubb, K.L., Trapnell, C., Fields, S., Queitsch, C., and Cuperus, J.T. (2019). Dynamics of Gene Expression in Single Root Cells of Arabidopsis thaliana. Plant Cell *31*, 993–1011.
34. Martin, B.D., Witten, D., and Willis, A.D. (2020). Modeling microbial abundances and dysbiosis with beta-binomial regression. Ann. Appl. Stat. *14*, 94–115.
35. Phipson, B., Sim, C.B., Porrello, E.R., Hewitt, A.W., Powell, J., and Oshlack, A. (2022). propeller: testing for differences in cell type proportions in single cell data. Bioinformatics *38*, 4720–4726.
36. Eberlein, S. (1985). Stage specific embryonic defects following heat shock in Drosophila. Dev. Genet. *6*, 179–197.
37. Johnston, I.A., Lee, H.-T., Macqueen, D.J., Paranthaman, K., Kawashima, C., Anwar, A., Kinghorn, J.R., and Dalmay, T. (2009). Embryonic temperature affects muscle fibre recruitment in adult zebrafish: genome-wide changes in gene and microRNA expression associated with the transition from hyperplastic to hypertrophic growth phenotypes. J. Exp. Biol. *212*, 1781–1793.
38. Diaz-Cuadros, M., Miettinen, T.P., Skinner, O.S., Sheedy, D., Díaz-García, C.M., Gapon, S., Hubaud, A., Yellen, G., Manalis, S.R., Oldham, W.M., and Pourquié, O. (2023). Metabolic regulation of species-specific developmental rates. Nature *613*, 550–557.

39. Bennett, J.T., Joubin, K., Cheng, S., Aanstad, P., Herwig, R., Clark, M., Lehrach, H., and Schier, A.F. (2007). Nodal signaling activates differentiation genes during zebrafish gastrulation. Dev. Biol. *304*, 525–540.

40. Ishikawa, T., Kashima, M., Nagano, A.J., Ishikawa-Fujiwara, T., Kamei, Y., Todo, T., and Mori, K. (2017). Unfolded protein response transducer IRE1-mediated signaling independent of XBP1 mRNA splicing is not required for growth and development of medaka fish. Elife *6*, e26845. https://doi.org/10.7554/eLife.26845.

41. Ishikawa, T., Okada, T., Ishikawa-Fujiwara, T., Todo, T., Kamei, Y., Shigenobu, S., Tanaka, M., Saito, T.L., Yoshimura, J., Morishita, S., et al. (2013). ATF6α/β-mediated adjustment of ER chaperone levels is essential for development of the notochord in medaka fish. Mol. Biol. Cell *24*, 1387–1395.

42. Ishikawa, T., Toyama, T., Nakamura, Y., Tamada, K., Shimizu, H., Ninagawa, S., Okada, T., Kamei, Y., Ishikawa-Fujiwara, T., Todo, T., et al. (2017). UPR transducer BBF2H7 allows export of type II collagen in a cargo- and developmental stage-specific manner. J. Cell Biol. *216*, 1761–1774.

43. Iwakoshi, N.N., Lee, A.-H., Vallabhajosyula, P., Otipoby, K.L., Rajewsky, K., and Glimcher, L.H. (2003). Plasma cell differentiation and the unfolded protein response intersect at the transcription factor XBP-1. Nat. Immunol. *4*, 321–329.

44. Angelos, E., and Brandizzi, F. (2022). The UPR regulator IRE1 promotes balanced organ development by restricting TOR-dependent control of cellular differentiation in Arabidopsis. Plant J. *109*, 1229–1248.

45. Pavitt, G.D., and Ron, D. (2012). New insights into translational regulation in the endoplasmic reticulum unfolded protein response. Cold Spring Harb. Perspect. Biol. *4*, a012278. https://doi.org/10.1101/cshperspect.a012278.

46. Yasuoka, Y. (2020). Morphogenetic mechanisms forming the notochord rod: The turgor pressure-sheath strength model. Dev. Growth Differ. *62*, 379–390.

47. Stemple, D.L., Solnica-Krezel, L., Zwartkruis, F., Neuhauss, S.C., Schier, A.F., Malicki, J., Stainier, D.Y., Abdelilah, S., Rangini, Z., Mountcastle-Shah, E., and Driever, W. (1996). Mutations affecting development of the notochord in zebrafish. Development *123*, 117–128.

48. Gansner, J.M., and Gitlin, J.D. (2008). Essential role for the alpha 1 chain of type VIII collagen in zebrafish notochord formation. Dev. Dyn. *237*, 3715–3726.

49. Griffin, K.J., Amacher, S.L., Kimmel, C.B., and Kimelman, D. (1998). Molecular identification of spadetail: regulation of zebrafish trunk and tail mesoderm formation by T-box genes. Development *125*, 3379–3388.

50. van Oosten-Hawle, P., Porter, R.S., and Morimoto, R.I. (2013). Regulation of organismal proteostasis by transcellular chaperone signaling. Cell *153*, 1366–1378.

51. Prahlad, V., Cornelius, T., and Morimoto, R.I. (2008). Regulation of the cellular heat shock response in Caenorhabditis elegans by thermosensory neurons. Science *320*, 811–814.

52. Morgan, R., Finnøen, M.H., Jensen, H., Pélabon, C., and Jutfelt, F. (2020). Low potential for evolutionary rescue from climate change in a tropical fish. Proc. Natl. Acad. Sci. USA *117*, 33365–33372.

53. Trapani, V., Bonaldo, P., and Corallo, D. (2017). Role of the ECM in notochord formation, function and disease. J. Cell Sci. *130*, 3203–3211.

54. Köhler, A., Mörgelin, M., Gebauer, J.M., Öcal, S., Imhof, T., Koch, M., Nagata, K., Paulsson, M., Aumailley, M., Baumann, U., et al. (2020). New specific HSP47 functions in collagen subfamily chaperoning. FASEB J. *34*, 12040–12052.

55. Cagnetta, R., Wong, H.H.-W., Frese, C.K., Mallucci, G.R., Krijgsveld, J., and Holt, C.E. (2019). Noncanonical Modulation of the eIF2 Pathway Controls an Increase in Local Translation during Neural Wiring. Mol. Cell *73*, 474–489.e5.

56. Hetz, C., and Mollereau, B. (2014). Disturbance of endoplasmic reticulum proteostasis in neurodegenerative diseases. Nat. Rev. Neurosci. *15*, 233–249.

57. Hollien, J. (2013). Evolution of the unfolded protein response. Biochim. Biophys. Acta *1833*, 2458–2463.

58. Andreatta, M., Corria-Osorio, J., Müller, S., Cubas, R., Coukos, G., and Carmona, S.J. (2021). Interpretation of T cell states from single-cell transcriptomics data using reference atlases. Nat. Commun. *12*, 1–19.

59. Yee, T.W. (2010). The VGAM Package for Categorical Data Analysis. J. Stat. Softw. *32*, 1–34.

60. Concordet, J.-P., and Haeussler, M. (2018). CRISPOR: intuitive guide selection for CRISPR/Cas9 genome editing experiments and screens. Nucleic Acids Res. *46*, W242–W245.

61. Hoshijima, K., Jurynec, M.J., Klatt Shaw, D., Jacobi, A.M., Behlke, M.A., and Grunwald, D.J. (2019). Highly Efficient CRISPR-Cas9-Based Methods for Generating Deletion Mutations and F0 Embryos that Lack Gene Function in Zebrafish. Dev. Cell *51*, 645–657.e4.

STAR★METHODS

KEY RESOURCES TABLE

REAGENT or RESOURCE	SOURCE	IDENTIFIER
Chemicals, peptides, and recombinant proteins		
20% Paraformaldehyde Aqueous Solution, EM Grade	EMS	50-980-492
Collagenase P	Millipore-Sigma	11213865001
1X TrypLE Express	Thermo Fisher	12604013
DPBS, no calcium, no magnesium	Thermo Fisher	14190144
SUPERase In RNase Inhibitor	Thermo Fisher	AM2696
BSA	NEB	B9000S
IGEPAL CA-630	Millipore Sigma	I8896
Triton X-100 for molecular biology	Millipore Sigma	T8787
Superscript IV reverse transcriptase	Thermo Fisher	18090200
RNaseOUT Recombinant Ribonuclease Inhibitor	Thermo Fisher	10777019
NEBNext High Fidelity 2x PCR master mix	NEB	M0541L
NEBNext mRNA Second Strand Synthesis Module	NEB	E6111L
Agencourt AMPure XP Beads	Beckman Coulter	A63882
N,N-Dimethylformamide	Millipore Sigma	D4551
Experimental models: Organisms/strains		
Zebrafish/Wild-type AB strain	U. Washington	N/A
Deposited data		
Raw FASTQ files	GEO	GEO: GSE202294
Processed count matrix	GEO	GSE202294
Cell metadata	GEO	GSE202294
Oligonucleotides		
Indexed reverse transcription oligos (5′-/5Phos/CAG AGCNNNNNNNN[10bpRTindex]TTTTTTTTTTTTTTT TTTTTTTTTTTTTT-3′)	IDT	https://cole-trapnell-lab.github.io/zscape/
Indexed ligation oligos (5′- GCTCTG[10bp barcode A]/ideoxyU/ACGACGCTCTTCCGATCT[reverse complement of barcode A]-3′)	IDT	https://cole-trapnell-lab.github.io/zscape/
Indexed PCR oligos (P5) (5′- AATGATACGGCGAC CACCGAGATCTACAC[i5]ACACTCTTTCCCTACAC GACGCTCTTCCG ATCT-3′)	IDT	https://cole-trapnell-lab.github.io/zscape/
Indexed PCR oligos (P7) (5′- CAAGCAGAAGACGG CATACGAGAT[i7]GTCTCGTGGGCTCGG-3′	IDT	https://cole-trapnell-lab.github.io/zscape/
Tn5-N7 oligo (5′-GTCTCGTGGGCTCGGAGATGTGT ATAAGAGACAG-3′)	Eurofins	N/A
Tn5 Mosaic End (ME) oligo (5′-/5Phos/CTGTCTCTT ATACACATCT-3′)	Eurofins	N/A
Software and algorithms		
Monocle 3 v1.3.1	This paper; Saunders et al.[32]	https://cole-trapnell-lab.github.io/monocle3/
R 4.1.3	CRAN	https://cran.r-project.org/
bbi-demux v1.0	Github	https://github.com/bbi-lab/bbi-dmux
bbi-sci v1.0	Github	https://github.com/bbi-lab/bbi-sci
Nextflow 20.07.1	Nextflow	https://www.nextflow.io/

RESOURCE AVAILABILITY

Lead contact

Further information and requests for resources and reagents should be directed to and will be fulfilled by the lead contact, Cole Trapnell (coletrap@uw.edu).

Materials availability

This study did not generate new unique reagents.

Data and code availability

- Single-cell RNA-seq data and raw sequencing are publicly available as of the date of publication via the NCBI Gene Expression Omnibus (GEO) accession GSE202294.
- All original code, including notebooks for performing data processing, statistical analysis and generating plots, has been deposited at Github and is publicly available as of the date of publication: https://github.com/cole-trapnell-lab/hotfish. Pipelines for generating count matrices from sci-RNA-seq3 sequencing data are available at https://github.com/bbi-lab/bbi-dmux and https://github.com/bbi-lab/bbi-sci. Analyses of the single cell transcriptome data were performed using Monocle3, which was updated to include methods from this study; a general tutorial can be found at http://cole-trapnell-lab.github.io/monocle-release/monocle3.
- All materials used in this study are available by request from the corresponding author.

EXPERIMENTAL MODEL AND STUDY PARTICIPANT DETAILS

Animals

Fish stocks used in this study were: wild-type AB. Adult fish were maintained at 28.5°C under 14 h:10 h light:dark cycles and fed daily. Embryo clutches were collected from several pairwise adult crosses. Embryos were shifted to elevated (32°C, 34°C, or 35°C) or reduced temperatures (20°C) at 6 hpf, and remained at these temperatures until sampling; staging followed Kimmel et al.[24] Embryos for this study were sampled between 24 hpf and 72 hpf. The sex of the embryos is not yet determined at stages profiled in this study. All procedures involving live animals followed federal, state and local guidelines for humane treatment and protocols approved by the Institutional Animal Care and Use Committee (protocol #2997-01) of the University of Washington.

METHOD DETAILS

Preparation of barcoded nuclei from individual embryos

Individual zebrafish embryos (24–36 hpf) were manually dechorionated and transferred to separate wells of a 96-well V-bottom plate containing 75 μL of 1X TrypLE + 2 mg/mL Collagenase P (Millipore Sigma, cat. 11213865001). Embryos were then dissociated manually at 30°C by pipetting every 5 min for about 20 min until no visible chunks were present under a dissecting scope. Stop solution (dPBS, 5% FBS) was then added to each well and cells were spun down at 600 x g for 5 min. Cells were then rinsed 1X in cold, 1X dPBS and spun down again. After rinses, supernatant was fully removed and cells were resuspended in 50 μL of cell lysis buffer (CLB) (Nuclei buffer, 0.1% IGEPAL, 1% SuperaseIn RNase Inhibitor (20 U/μL, Ambion), 1% BSA (20 mg/mL, NEB)) + hash oligos (1 μM, IDT) and incubated for 3 min on ice to liberate nuclei and integrate hash barcodes. To each well, 200 μL of ice-cold, 5% Paraformaldehyde was added to each well. After an additional round of mixing, nuclei were fixed on ice for 15 min. All wells were then pooled together in a 15 mL conical tube and spun down for 15 min at 750 x g. Supernatant was decanted and cells rinsed in 2 mL of cold NBB (Nuclei Buffer, 1% BSA, 1% SuperaseIn) at 750 x g for 6 min. Supernatant was then removed and cells were resuspended in 1 mL of NBB and flash frozen in LN2 and stored at −80.

Sci-RNA-seq3 library construction

The fixed nuclei were processed similarly to the published sci-RNA-seq3 protocol.[29] For paraformaldehyde fixed cells, frozen fixed cells were thawed on ice, spun down at 750 x g for 6 min, and incubated with 500 μL NBB (Nuclei buffer, 1% BSA, 1% SuperaseIn) including 0.2% Triton X-100 for 3 min on ice. Cells were pelleted and resuspended in 400 μL NBB. The cell suspension was sonicated on low speed for 12s. Cells were then pelleted at 750 x g for 5 min prior to resuspension in NB + dNTPs. The subsequent steps were similar with the sci-RNA-seq3 protocol (with paraformaldehyde fixed nuclei) with slight modifications: (1) We distributed 25,000 fixed cells (instead of 80,000 nuclei) per well for reverse transcription. (2) Centrifugation speeds for all spins were increased to 750 x g.

Sequencing, read processing and cell filtering

Libraries were sequenced on an Illumina Novaseq 6000 (S4 200 cycle kit) with sequencing chemistries compatible with library construction and kit specifications. Standard chemistry: I1 – 10 bp, I2 – 10 bp, R1 – 28 bp, R2 - remaining cycles (>45). Read alignment and gene count matrix generation was performed using the Brotman Baty Institute (BBI) pipeline for sci-RNA-seq3

(https://github.com/bbi-lab/bbi-sci). After the single cell gene count matrix was generated, cells with fewer than 200 unique molecular identifiers (UMIs) were filtered out. For mitochondrial signatures, we aggregated all reads from the mitochondrial chromosome. Each cell was assigned to a specific zebrafish embryo based on the total hash count (hash_umi $\geq$ 5) and the enrichment of a particular hash oligo (hash enrichment cutoff $\geq$ 3).

Count matrix pre-processing

Transcript by cell count matrix was pre-processed using a standard Monocle3 workflow: *estimate_size_factors()* - > *detect_genes (min_expr = 0.1)* - > *preprocess_cds()* with 100 principal components for whole-embryo and 50 principle components for subsets, *align_cds(residual_model_formula_str = "~log10(n.umi)")*, *reduce_dimension(max_components = 3, preprocess_method = 'Aligned')*, and finally *cluster_cells(resolution = 1e-4)*.

Cell annotation by projection of query data to reference

Cell type annotations were assigned via a label transfer procedure from the reference dataset (see Saunders et al.[32]) to the query temperature-treated dataset. Briefly, the PCA rotation matrix, log10(n.umi) batch correction linear model, and non-linear UMAP transformation from the reference data were computed and saved for subsequent transformation of query data. The query temperature-treated dataset was then projected into the reference space using the following procedure: coefficients to transformed gene expression values into PCA loadings were applied, the linear batch correction was then applied to remove effects of total UMIs per cell, and, lastly, the UMAP transformation was applied to the batch-adjusted PCA loadings to project query data into the reference coordinate space. A similar overall approach is used in Andreatta et al.[58]

After an initial transfer of the 'major group' label (four possibilities: mesoderm, mesenchyme-fin, periderm + other, CNS) in the global space of all cells, cells that gained major group labels were projected in a sub-space corresponding to that major group. In this sub-space, finer resolution annotations (germ layer, tissue, broad cell type, sub cell type) were transferred using the majority vote of reference neighbors (k = 10).

Estimation of transcriptional age for each cell and cell type

Alongside the process for transferring cell-type annotation labels as above, each cell from the query temperature-treated dataset was assigned an estimated time point label (mean_nn_time) by taking the average sample time point of its 10 nearest neighbors in the developmental reference dataset. For each embryo, we bulked and averaged all cells of the same type to compute a cell-type-specific ''transcriptional age.''

Comparison of embryo pseudostage with conventional staging

A linear model for the effects of temperature on developmental stage from Kimel et al. was used to generate stage expectations: h = H * (0.055T - 0.57), where h = hours of development to reach the stage at 28.5°C and H = hours of development at temperature T.[24]

Additive model for cell-type-specific acceleration

Signatures scores were computed using the *aggregate_gene_expression()* function in Monocle3, using the log-normalized average counts across gene sets representing several biological processes (Table S3C). To assess the baseline contributions of each process to acceleration by temperature, signature scores were computed for embryos raised at the standard 28°C. A linear model was used (vglm from VGAM package[59]) to examine the relationship of each signature with relative developmental acceleration, and coefficients for each process were compared.

Perturbation of proteostasis via CRISPR-Cas9 mutagenesis and inhibitors

gRNAs were designed using either the IDT or CRISPOR[60] online tool. gRNAs were synthesized by IDT as crRNAs, annealed to tracrRNAs and assembled into RNPs with spCas9 protein (IDT). Preparation and subsequent injection of RNPs was performed as previously described[61]; two gRNAs were simultaneously injected for *atf6.* To inhibit protein synthesis globally, embryos were treated with a non-lethal dose of 5 μM CHX (Sigma, C4859) starting at 6 hpf. To inhibit the UPR, embryos were treated with 100 μM ISRIB (Sigma, SML0843) starting at 6 hpf.

Transmission electron microscopy

Fish were euthanized then fixed in sodium cacodylate buffered 4% glutaraldehyde overnight at 4°C. Embryos were stained in 2% osmium tetroxide for 30 min, washed, and then stained in 1% uranyl acetate overnight at 4°C. Samples were dehydrated with a graded ethanol series then infiltrated with a 1:1 propylene oxide:Durcupan resin for 2 h followed by fresh Durcupan resin overnight and flat embedded prior to polymerization. Blocks of posterior tissue, from yolk extension to tail, were thin sectioned on a Leica EM UC7 and sections imaged on a JEOL 1230 transmission electron microscope.

Notochord staining

Alcian blue staining followed an online procedure (SDB Online Short Course, Zebrafish Alcian blue), except that embryos were raised in 1-phenyl-2-thiourea to suppress pigment formation instead of bleaching.

Differential gene expression analysis

To capture biological variation in gene expression between stage-matched embryos, cells of each type were first pseudobulked (sums of size-factor-normalized gene counts) by embryo. Using this embryo-level pseudobulk data as input, differentially expressed genes were determined in each cell type using the fit_models() function in Monocle3. The model formula included additive terms for temperature (as a factor), a spline of embryo pseudostage (degrees of freedom = 3), and the total number of cells. Global analysis of temperature-dependent gene expression was performed by extracting temperature coefficients from the model output, filtering for genes with significant q-values ($q < 0.05$). Temperature coefficients in each cell type were combined into a single matrix, and processed analogously to the find_gene_modules() function in Monocle3,[29] which uses a transposition of the typical gene x cell matrix to group genes with similar patterns across cells, rather than grouping cells. Temperature coefficients (no normalization) were preprocessed with PCA and dimensionality reduction was performed with UMAP (n_neighbors = 25L, min_dist = 0.2). Clusters of genes with similar temperature responses across cell types were identified using the cluster_cells() function.

Hotspot analysis

The local spatial statistic Getis-Ord index (G_i) was used to identify statistically significant regions of the UMAP embedding that were enriched or depleted of perturbed cells. A high-value G_i indicates that a perturbed cell is surrounded by other cells with the same perturbation, whereas a G_i close to zero indicates that a perturbed cell is surrounded by cells with other perturbation labels. A G_i was calculated for each cell's local neighborhood (k = 15) using the "localG()" function in the spdep package. This returns a *Z* score that indicates whether the observed spatial clustering is more pronounced than expected by random. Multiple testing correction was done using a Bonferroni correction. Areas of the UMAP where a given perturbation is enriched are called "hot spots."

QUANTIFICATION AND STATISTICAL ANALYSIS

$$\text{logit}(\mu_{i,t}) = \beta_t + \beta_{g,t}x_g$$

$$\text{logit}(\rho_{i,t}) = \chi_t + \chi_{g,t}x_g$$

$$y_{i,t} = \text{BeBin}(\mu_{i,t}, \rho_{i,t})$$

Cell abundance and variance statistics

Changes in the proportions of each cell type were assessed by first counting the number of each annotated cell type in each embryo. To control for technical differences in cell recovery across embryos, "size factors" by dividing the total number of cells recovered from an embryo by the geometric mean of total cell counts across all embryos. The number of cells of each type recovered from each embryo were then divided by that embryo's size factor. No explicit sample-size calculation was performed for number of embryos, but individual-embryo protocols were optimized to sample enough cells to capture all major cell types in the embryo between 24 and 96 hpf. No individual samples were excluded. Within samples, we excluded cells that did not pass quality filters from subsequent single-cell analysis; these include minimum UMI counts, mitochondrial read fraction, and doublets. No explicit randomized design was deployed, but individual replicate embryos were pooled and processed together, reducing technical batch effects. No blinding was used in this study.

Normalized counts for each cell type at different developmental stages were then compared across treatments using a generalized linear model defined by the equations:

Where the normalized counts of cell type at time is modeled as a beta-binomially distributed random variable with mean and overdispersion with respect to the binomial distribution. We modeled both parameters of the beta binomial response as a function of temperature, reasoning that treated embryos might exhibit greater variability than wild-type embryos. The binary indicator variable denotes treatment in each embryo. Separate models for each temperature in each cell type and at each pseudostage bin were fit using the VGAM package.[59] Significance of temperature effects in each model were assessed by a Wald test. In all figures, relevant comparisons and total values of *n* is denoted in figure legends.

ADDITIONAL RESOURCES

A website containing 3-level, individual-embryo indexing sci-RNA-seq protocol, as well as additional resources for visualizing wild-type and temperature-treated atlases can be found at: https://cole-trapnell-lab.github.io/zscape/.

CellPress
OPEN ACCESS

Supplemental figures

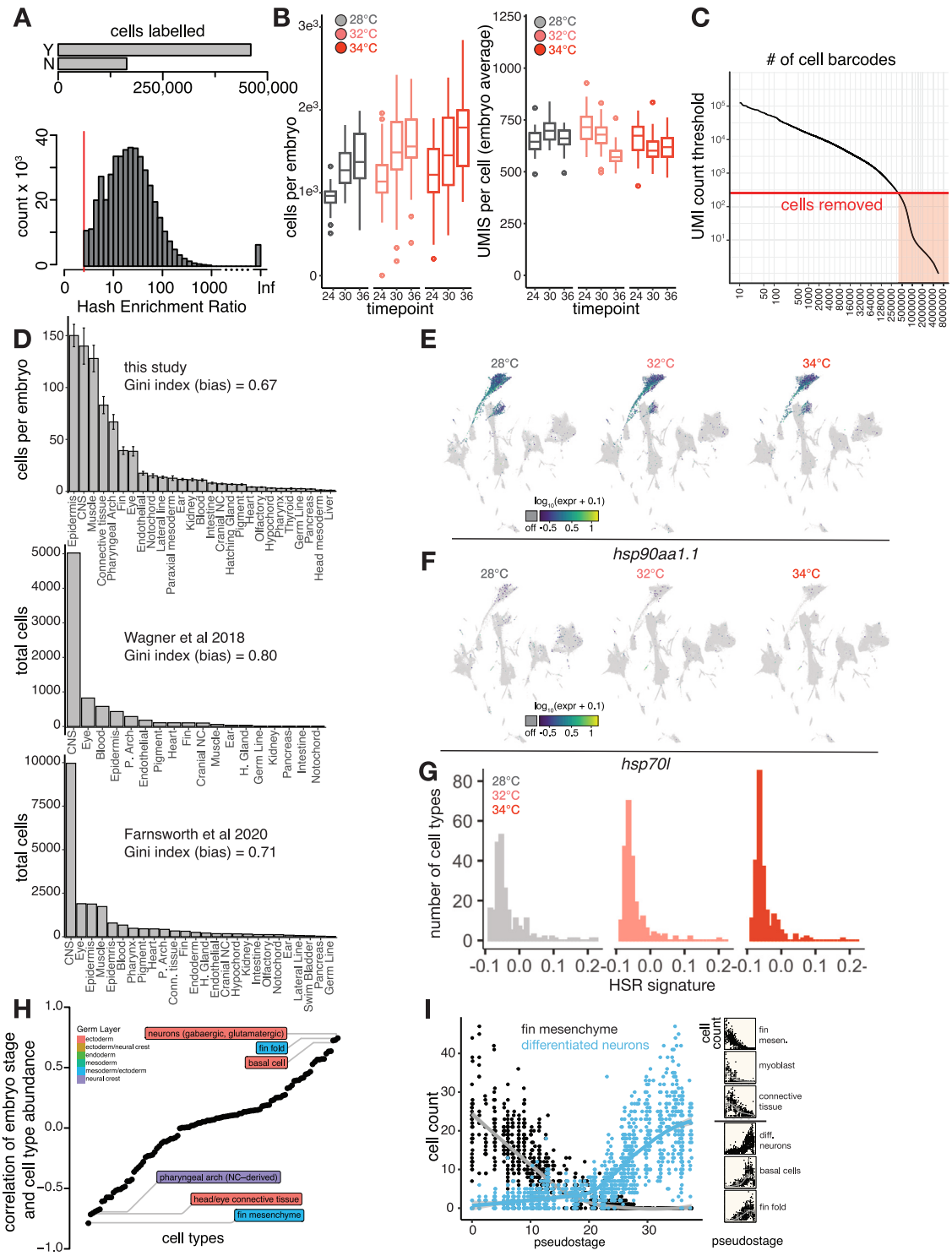

(legend on next page)

Figure S1. Individual-level capture of high-quality single-cell transcriptomes, related to Figure 1

(A) Bar plot showing the number of individual cells that pass (Y, yes; N, no) a hash enrichment ratio (count of most abundant hash relative to second-most abundant) threshold of 3. Below is a histogram showing the full distribution of hash enrichment ratios; cells where all reads were derived from a single hash are labeled as "Inf."

(B) Box plots showing the number of cells in each embryo (left) and number of UMIs per cell in each embryo (right), faceted by sample time point and colored by temperature treatment.

(C) Knee plot showing the threshold for UMI count (red line) in called cells.

(D) Bar plots showing tissue compositions as per-embryo cell counts in two additional single-cell RNA-seq studies of zebrafish whole-embryo samples. A measure of composition bias (Gini index) is listed above each bar chart; higher values indicate higher bias in tissue recovery or less even coverage across tissues.

(E) Marker plot showing no induction of hsp90aa1.1 at 32°C or 34°C, including cells from all time points.

(F) Marker plot for hsp70L, a gene used for transgenic reporters of heat shock in zebrafish, shown as in (E).

(G) Histogram showing no systemic activation of the HSR across cell types at any of the temperatures profiled. While the total number of cell types with negligible HSR levels increases with temperature, nearly all cell types should have HSR signature values greater than 0 in the event of global activation of the HSR.

(H) Dot plot of each cell type, ordered by the Pearson correlation between that cell type's abundance and the whole-embryo pseudostage. Bellwether cell types with the highest correlations are labeled, with colors indicating tissue of origin.

(I) Two examples from the highly correlated types shown in (A), with raw cell-type abundance data plotted against embryo stage for a strong negatively correlated type (fin mesenchyme) and strong positively correlated type (differentiated neurons); inset at right shows additional examples.

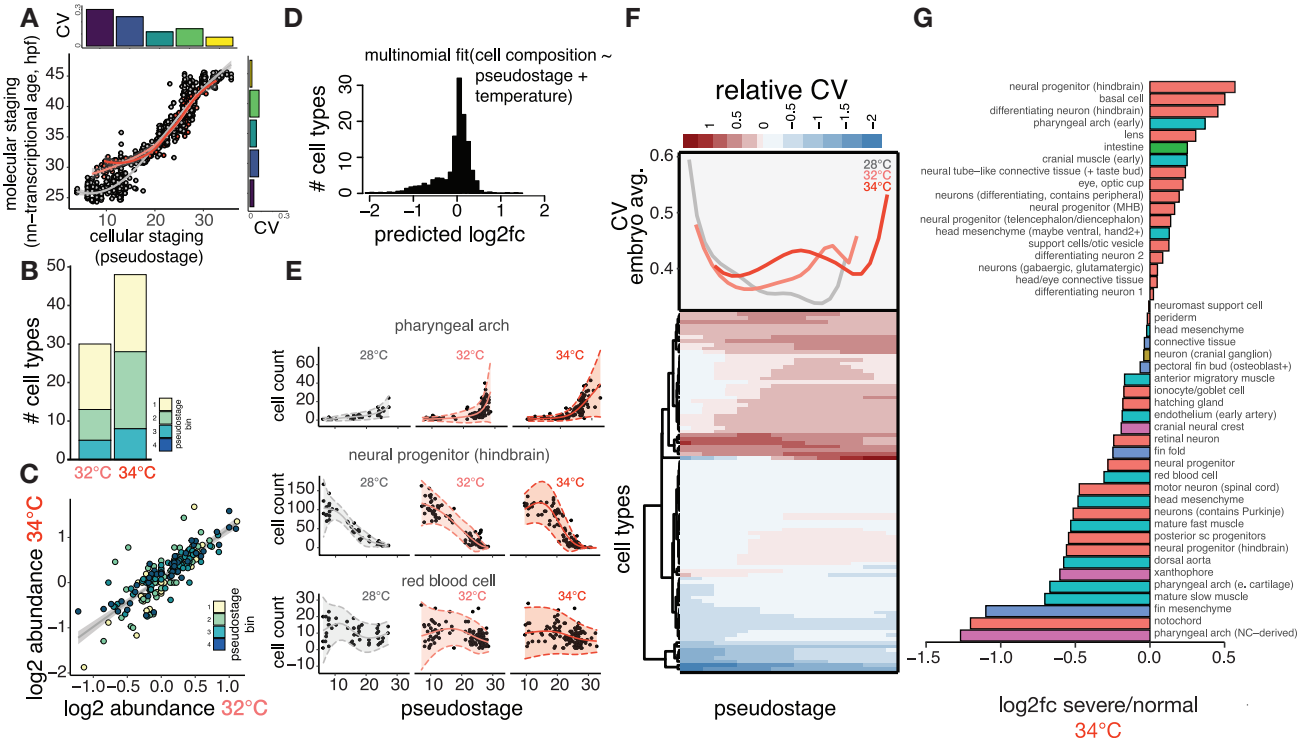

Figure S2. Temperature increases variability in specific cell types and stages of development, related to Figure 2

(A) Scatterplot comparing whole-embryo staging determined by either cell composition (x axis) or transcriptional data (y axis); inset bar plots show CV for each metric in groups of embryos sampled at various time points (time points in hpf indicated in gray text above each bar). Loess fit lines are shown for embryos raised at each temperature: 28°C (gray), 32°C (pink), and 34°C (red).

(B) Stacked bar chart showing how the number of cell types with significant abundance changes increases with temperature; this phenomenon held for all pseudostage bins (in color) except bin 4, which lacked sufficient control embryos to analyze statistically.

(C) Scatterplot showing positive relationship of log2 fold change in abundances in both elevated temperatures, colored as in (A).

(D) Histogram showing changes in cell composition resulting from 34°C treatment, as predicted by multinomial model.

(E) Scatterplots showing raw data (black points) and model outputs of mean (solid line) and variability (ribbons with dotted line) for three temperature-sensitive cell types.

(F) Heatmap of each cell type showing relative increases in observed variability compared with variability expected during wild-type development through developmental time (pseudostage bins); shades of red indicate increased variability, while white to blue shades show neutral or decreased variability. The upper panel shows the average CVs for each temperature across all stages, highlighting pseudostages with increased variability at higher temperatures.

(G) Bar plot showing the log2 fold change in abundance for all cell types in 34°C embryos with severe phenotypes relative to those that were phenotypically normal

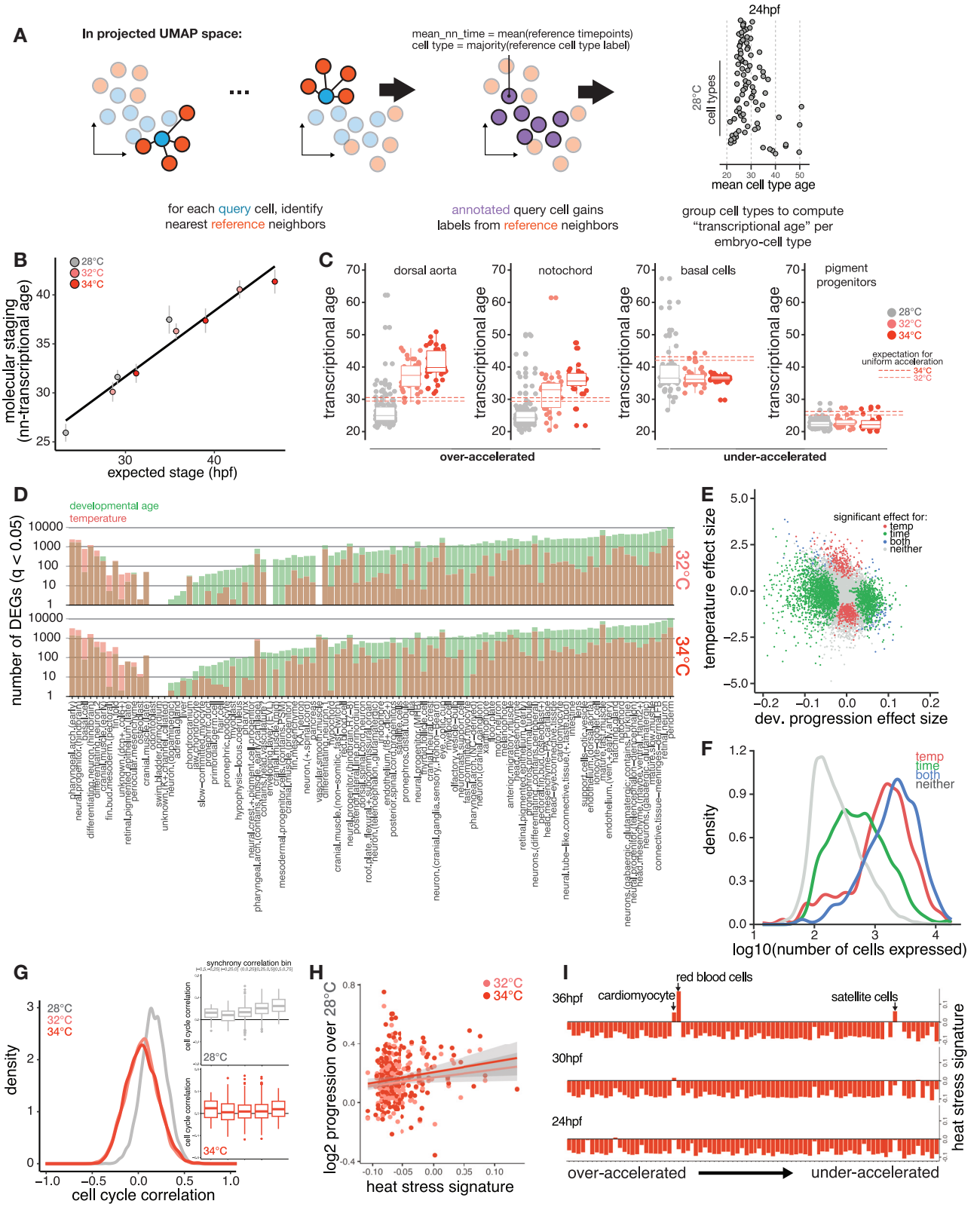

(legend on next page)

Figure S3. Temperature accelerates development non-uniformly across cell types, related to Figure 3

(A) Schematic showing method for computing transcriptional age of each cell through nearest-neighbor averaging of time point labels in the reference.

(B) Scatterplot as in Figure 2B but showing how well whole-embryo staging by transcriptional data (nn-transcriptional age), rather than cell composition, predicts temperature-induced developmental acceleration.

(C) Boxplots showing individual examples of cell types with greater-than-expected acceleration (left) and less-than-expected acceleration (right), with whole embryo expectation from Kimmel et al.[24] for each temperature shown as dotted lines.

(D) Bar plots showing the number of significantly ($q < 0.05$) differentially expressed genes in each cell type, separated by whether the gene has a significant association for developmental age (green) or temperature (red). Cell types along the x axis are ordered by the difference between the number of significant temperature genes vs. significant developmental age genes; the large majority shows more genes changing with developmental age rather than temperature.

(E) Scatterplot showing significant genes separated by developmental age and temperature effects for a specific cell type, the notochord. Temperature and age coefficients are shown for each gene and are colored based on significant associations with each factor, neither, or both.

(F) Density histogram showing that genes with significant associations with temperature tended to show higher expression levels than developmental age genes.

(G) Density histogram of pairwise Pearson correlations for cell-cycle signature values across all cell-type pairs, with separate densities for each temperature. Inset shows boxplots of pairwise cell-cycle correlations grouped into cell-type pairs that showed lower or higher levels of developmental timing synchrony.

(H) Scatterplot, as in Figure 3C, showing that the basal level of HSR signature in each cell type is not a strong predictor of that cell type's developmental acceleration at 32°C or 34°C.

(I) Bar plots showing the level of HSR signature induction for all cell types at 34°C; cell types on the y axis are ordered by relative developmental acceleration, with the most strongly accelerated types at the top, and columns for each time point. No induction of HSR signature is apparent in the most accelerated cell types.

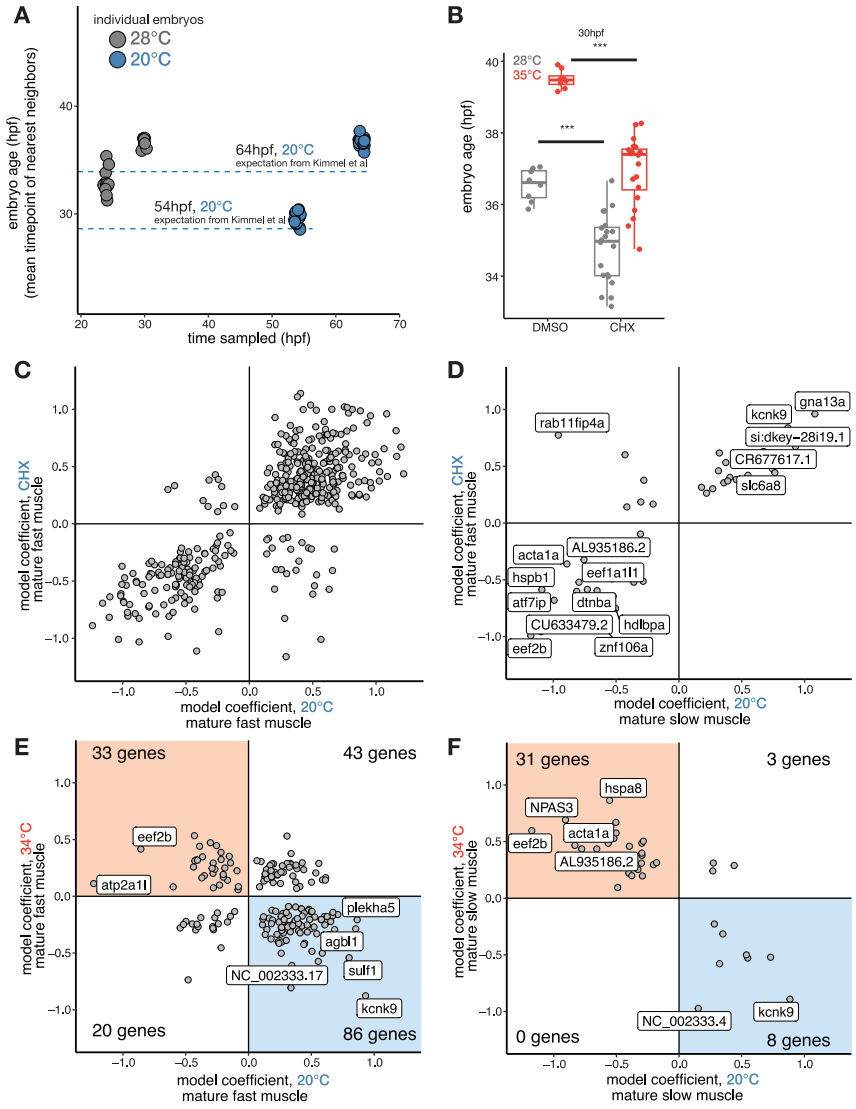

Figure S4. Cold treatment slows development and reveals cell-type-specific temperature-responsive genes in the normal range of zebrafish development, related to Figure 3

(A) Dot plot showing the sampling timing for cold-treated embryos (x axis is clock time), as well as their predicted whole-embryo stage based on integration with the 28°C reference data; the predicted stage roughly matched the expectation of the Kimmel et al.[24]

(B) Boxplot showing the effect of 5 μM CHX on temperature-induced acceleration of whole-embryo stage; developmental delay is evident in CHX-treated embryos raised at 28°C, and this effect is not overridden by 34°C temperature treatment.

(C) Scatterplot showing temperature-dependent activation of genes of the fast muscle, expressed as model coefficients for each temperature after accounting for developmental stage. Most genes showed either heat-induced increases and cold-induced decreases in expression (red box in upper left) or heat-induced decreases and cold-induced increases in expression (blue box in lower left).

(D) Scatterplot as in (C), but for slow muscle.

€ Scatterplot for fast muscle similar to (B) but showing cold vs. CHX treatment, which shows an overall strong positive correlation with gene expression similarly affected by both sources of developmental delay.

(F) Scatterplot as €(E), but for slow muscle.

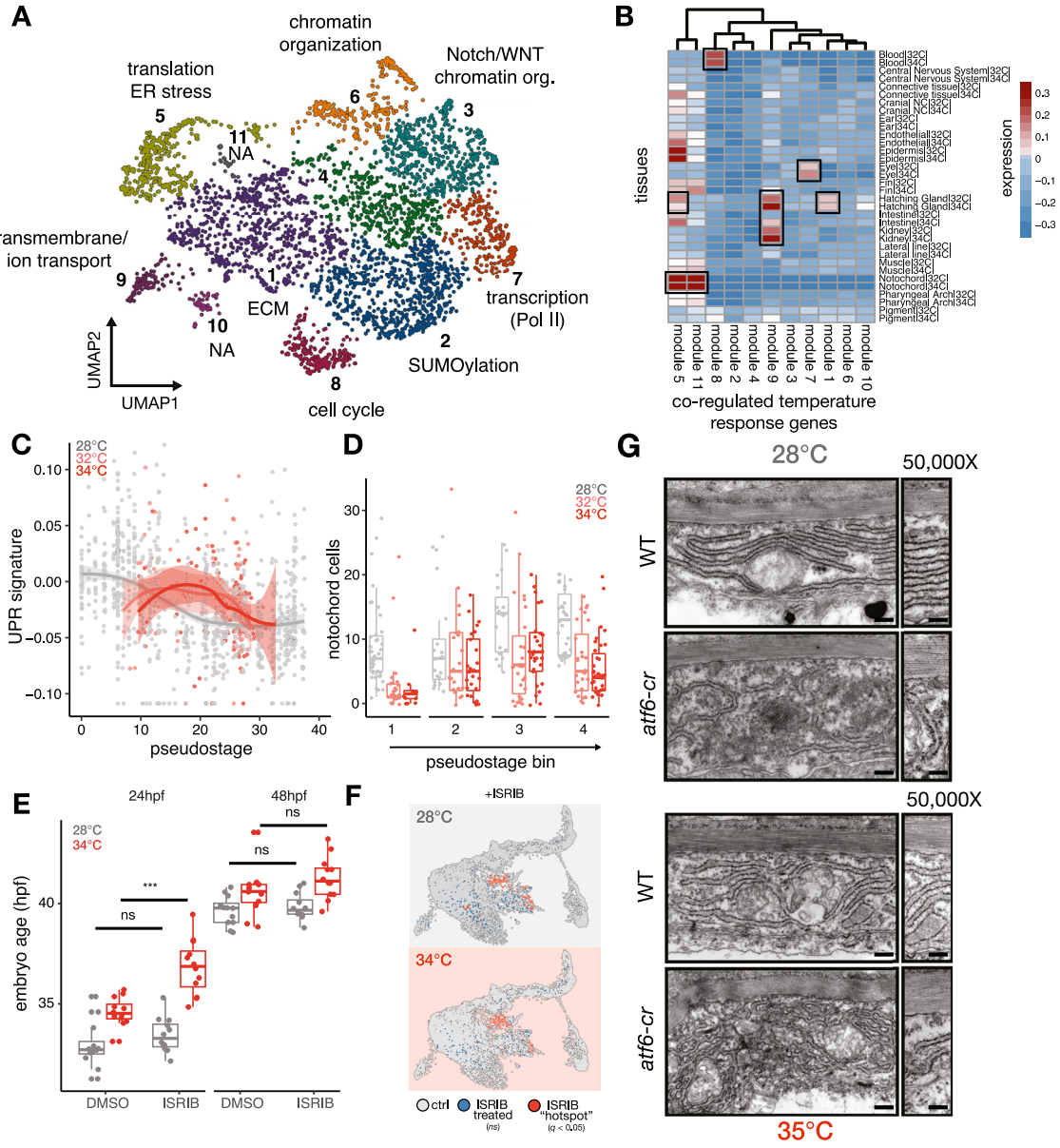

Figure S5. Transcriptional responses to elevated temperature tend to be cell-type-specific, revealing burdens on proteostasis in the notochord, related to Figure 4

(A) UMAP of all genes with significant temperature-dependent transcriptional changes (see STAR Methods). Each point represents an individual gene, and genes with similar responses (coefficient in differential expression model after accounting for stage) across cell types are grouped together. Each cluster is labeled with a different color, and a representative Gene Ontology (GO) term for the group of genes in each cluster is indicated. Clusters in which gene groups returned no significant GO terms are labeled "NA."

(B) Heatmap of expression levels for each gene module in (A) as an average for each cell type at elevated temperatures. Consistent with the heterogeneous grouping of temperature responses in (A), elevated module expression tends to be cell-type specific (examples boxed). Module 5, which contains genes related to translation and ER processing, has the broadest response across cell types, but the magnitude of the response is greatest within the notochord.

(C) Scatterplot showing levels of UPR signature in the notochord cells of all individual embryos, colored by temperature. Embryos raised at higher temperature show higher levels of UPR signature at nearly all profiled stages. Lines and ribbons are derived from LOESS fits across pseudostage.

(D) Boxplot showing marked reduction of notochord cells in embryos raised at high temperature, with raw counts in control and temperature-treated embryos shown as poi€.

(E) Boxplot showing the effect of the UPR inhibitor ISRIB on whole-embryo stage at 28°C and 34°C; embryos treated with ISRIB showed significant increases over expected temperature-induced acceleration at 24 hpf, but this effect was not evident in 48 hpf embryos.

(legend continued on next page)

(F) Hotspot analysis, as in Figure 4D, showing enriched transcriptional state of notochord sheath cells in embryos treated with ISRIB; note that ISRIB-treated cells do not occupy the high-temperature state identified in wild-type embryos.
(G) TEM of sheath cells in wild-type and *atf6* crispants showing effects in both untreated and temperature-treated embryos. ER structure is perturbed in *atf6* crispants, and severe sheath defects are visible in the temperature-treated *atf6* crispants. Scale bar, 200 nm.